minerals

MDPI

Article

Subduction–Accretion History of the Paleo-Pacific Plate Beneath the Eurasian Continent: Evidence from the Tongjiang Accretionary Complex, NE China

Bingying Du [1,2], Chenglu Li [3,*], Fei Liu [4,*], Tianjia Liu [5], Yuwei Liu [2], Xunlian Wang [1], Yong Liu [4] and Tiean Zhang [2]

[1] School of the Earth Sciences and Resources, China University of Geosciences (Beijing), Beijing 100083, China; hljdubingying@126.com (B.D.); wxl@cugb.edu.cn (X.W.)
[2] Heilongjiang Province Geological Science Institute, Harbin 150036, China; kill_vv@163.com (Y.L.); zhangtiean@sina.com (T.Z.)
[3] Natural Resources Survey Institute of Heilongjiang Province, Harbin 150036, China
[4] The Institute of Geology, Chinese Academy of Geological Sciences, Beijing 100037, China; liuyongfirst@163.com
[5] Petroleum Exploration and Production Research Institute, SINOPEC, Beijing 100083, China; tianjia@email.cugb.edu.cn
* Correspondence: lcl230881@163.com (C.L.); lfhy112@126.com (F.L.)

Abstract: Detrital zircons in the matrix of an accretionary complex play an important role in providing evidence to reconstruct oceanic plate subduction and accretion processes. The Nadanhada accretionary complex (NAC) dominated by the Yuejinshan, Raohe and Tongjiang accretionary complexes provides significant geological evidence to better understand the Paleo-Pacific subduction–accretion process. Most previous studies have focused on the Yuejinshan and Raohe accretionary complexes, while those of the Tongjiang accretionary complex on the north side have focused on blocks. In this study, we present zircon U–Pb dating and Hf isotopic data for the matrix of metasedimentary rock in the Tongjiang accretionary complex. The analysis results show that the zircons in the fine silty mudstone, phyllonite and fine argillaceous siltstone define the youngest weighted mean ages (youngest detrital zircon ages) of 261.4 ± 2.9 Ma (247 Ma), 175.2 ± 4.9 Ma (169 Ma) and 168.6 ± 2.1 Ma (162 Ma), respectively, and yield a younging trend of the accretion materials from west to east. Provenance analysis indicates that the matrix was mainly sourced from the neighboring Jiamusi and Xingkai blocks. Based on previous results of the Permian and Late Triassic blocks in the Yuejinshan region, the Permian and Early Jurassic blocks in the Tongjiang region, and the Late Triassic and Early–Middle Jurassic blocks in the Raohe region, as well as the lower limit of the depositional age of the Late Triassic matrix in the Yuejinshan region and the Middle Jurassic and Early Cretaceous matrices in the Raohe region, we propose that the NAC may record the Late Permian–Triassic, Jurassic and Early Cretaceous oceanic accretion events, representing the westward subduction and accretion process of the Paleo–Pacific Ocean Plate.

Keywords: Tongjiang region; subduction accretive complex; detrital zircon U–Pb ages; Hf isotope; Paleo–Pacific Plate

check for updates

Citation: Du, B.; Li, C.; Liu, F.; Liu, T.; Liu, Y.; Wang, X.; Liu, Y.; Zhang, T. Subduction–Accretion History of the Paleo-Pacific Plate Beneath the Eurasian Continent: Evidence from the Tongjiang Accretionary Complex, NE China. *Minerals* **2023**, *13*, 1038. https://doi.org/10.3390/min13081038

Academic Editor: Rubén Díez-Fernández

Received: 10 June 2023
Revised: 23 July 2023
Accepted: 31 July 2023
Published: 3 August 2023

Copyright: © 2023 by the authors. Licensee MDPI, Basel, Switzerland. This article is an open access article distributed under the terms and conditions of the Creative Commons Attribution (CC BY) license (https://creativecommons.org/licenses/by/4.0/).

1. Introduction

The accretionary complex represents the vestiges of the extinction of the Paleo–oceanic basin and records the history of the tectonic evolution between oceanic and continental plates. It provides important insights into the structure of accretion–type orogen and the evolutionary history of the ocean basin and offers direct evidence for reconstructing the subduction and accretion process of the oceanic plate [1–7]. Northeast (NE) China is situated at the intersection of the Siberia Craton, the North China Craton and the Pacific Plate. The accretionary complex in NE China records the subduction and accretion processes of the

Paleo–Asian Ocean and Paleo–Pacific Ocean [8–10]. The transition between the Paleo-Asian oceanic regime and the Paleo-Pacific regime, the initial timing of subduction, and the subduction and accretion process of the Paleo-Pacific Plate beneath the Eurasian continent remain controversial [11–15]. Different arguments have been proposed to constrain the initial subduction in the Early Jurassic [15–19], Late Triassic [11,20] or Permian [21,22]. The Nadanhada accretionary complex (NAC) is located in the easternmost region of NE China and is separated from Sikhote–Alin Mountain by the Wusuli River. This accretionary complex is an important component of the Wandashan–Sikhote–Alin accretionary complex belt and provides direct materiel records of the subduction and accretion of the Paleo–Pacific Plate beneath the Eurasian continent [12,14,20,23–28]. Thus, the NAC is a significant region for studying these geological problems.

The NAC is divided into the Yuejinshan Complex in the west and the Raohe Complex in the east [12,14,20,27,29,30] and sporadically outcrops in the Tongjiang–Fuyuan region. The nature and formation age of the Paleo–oceanic basin represented by the Yuejinshan accretionary complex remains in dispute. Existing studies argue for the subduction–accretion products of the Paleo–Asian Ocean [15,31], Paleo–Pacific Ocean [20,21,32] or Panthalassa [30,33,34] and the formation age of the late Late Paleozoic [15,34] or the Late Triassic–Early Jurassic [12,14,20]. The Raohe accretionary complex is generally considered to represent an accretionary complex formed by the subduction of the Paleo–Pacific Plate beneath the Eurasian continent [15,34–36]. The matrix has a progressively younging trend from west to east with ages ranging from the Middle Jurassic to Early Cretaceous, which is modelled as the westward subduction and accretion process of the Paleo–Pacific Plate [12,14,20,25]. However, based on detrital zircon dating of the Middle–Upper Jurassic Dalingqiao Formation in the Raohe region, other studies have suggested that there is no younging trend from west to east [37]. In addition, different viewpoints on the formation background of the Permian igneous rocks in the Jiamusi Block have proposed the subduction of the Paleo–Asian Ocean [38,39], Mongol–Okhotsk Ocean [40,41], Paleo-Pacific Ocean [22,42–44] or Panthalassa [30]. In summary, the orogenesis of the NAC and the continental marginal island arc on the west side are still controversial. This has resulted in debate on the initial timing of the subduction of the Paleo–Pacific Plate beneath the Eurasian continent, and a variable initial timing of the Early Jurassic [15,17–19], Late Triassic [20,34] or Permian [21,22,45] have been proposed. The NAC is a significant region in NE China for understanding the subduction and accretion process of the Paleo–oceanic basin. However, the process recorded by the NAC is still unclear.

The Tongjiang accretionary complex is situated in the northwestern part of the NAC and is separated from the Raohe and Yuejinshan accretionary complexes by the Cenozoic basin. The matrix includes siltstone, argillaceous siltstone, silty mudstone and phyllonite, and ductile deformation is developed locally. The block includes pyroxenite, siliceous rock, gabbro, basalt, andesite and rhyolite, which are commingled in the matrix. Lenticular blocks occur in the matrix, with various sizes ranging from tens of centimeters to hundreds of meters. Most previous studies have focused on the geochemical and geochronological data of the block in the Tongjiang accretionary complex [18,32,46,47] with a lack of geochronological study of its matrix. Thus, field geological investigation, zircon geochronology and Lu–Hf isotope analysis of the matrix in the Tongjiang accretionary complex were integrated in this study to constrain the age and provenance of the matrix. Based on the age and provenance analysis results of the matrix in this study and combined with previous research studies, we hypothesized that the NAC is the product of the subduction and accretion of the Paleo–Pacific Plate; we also aimed to reconstruct the subduction and accretion process of the Paleo–Pacific Plate beneath the Eurasian continent.

2. Regional Setting

Northeast (NE) China is located in the eastern Central Asian Orogenic Belt and has experienced superposition of the Paleo-Asian Ocean, Mongol–Okhotsk Ocean and Paleo–Pacific Ocean tectonic regimes [11,13,34]. The region is characterized by several micro–

continental blocks, accretionary complexes and arc basins and records the accretionary orogenic process of the Xing-Meng Orogenic Belt. The Xing–Meng Orogenic Belt is situated between the Siberian Craton to the north and the North China Craton to the south and is the amalgamation of several micro–continental blocks [9,13,48]. It can be divided into five micro–continental blocks from west to east: the Erguna Block, the Xing'an Block, the Songliao Block, the Jiamusi Block and the Xingkai Block (Figure 1a) [9,13,49].

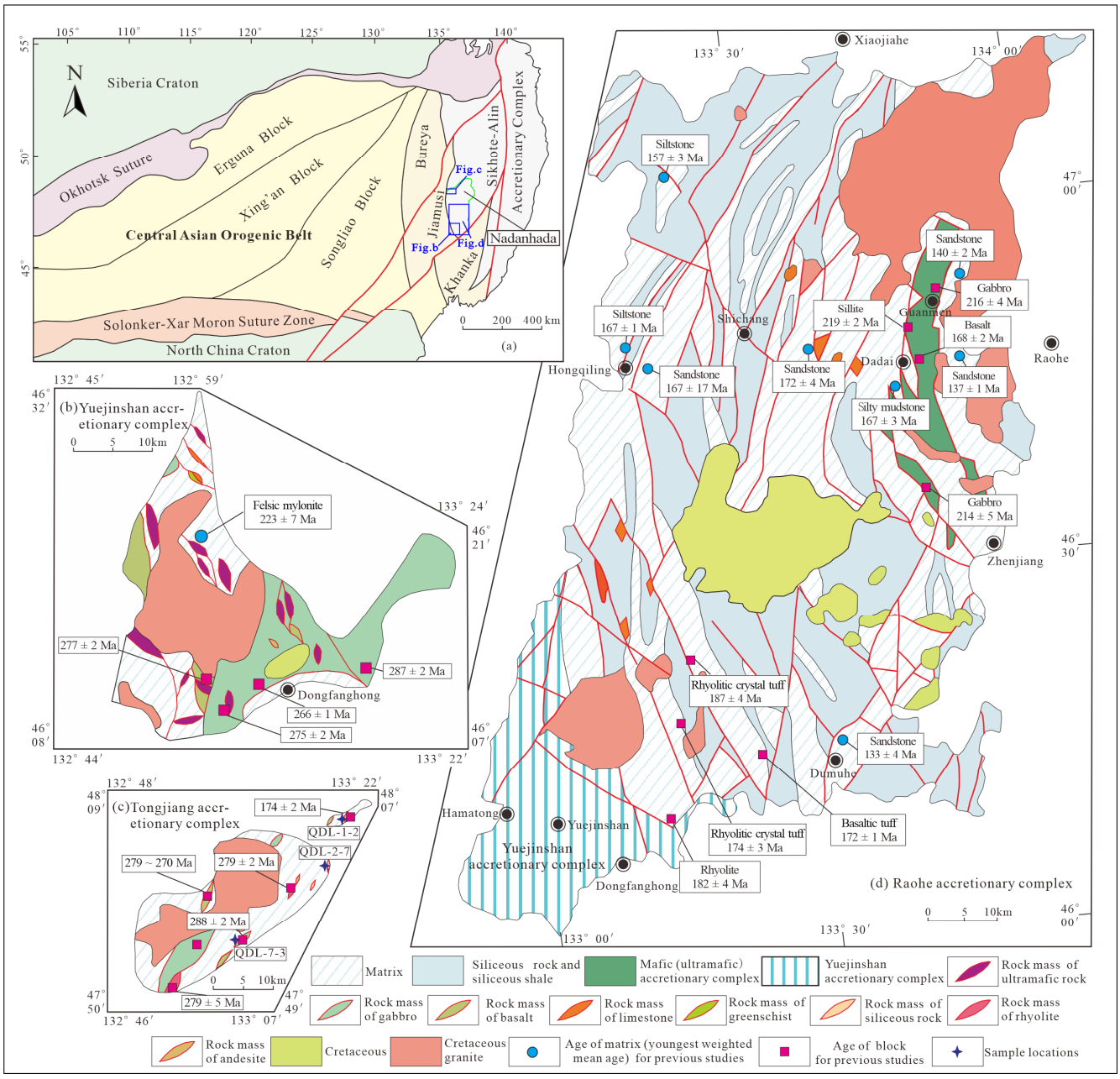


Figure 1. (**a**) Simplified map of the division of tectonic units in Northeast China and adjacent regions [21]; (**b**) Geological map of the Yuejinshan accretionary complex; (**c**) Geological map of the Tongjiang accretionary complex [50]; (**d**) Geological map of the Raohe accretionary complex [20] (The ages were obtained from [14,18,20,21,32,33,35,44,51–55] and references therein).

The NAC is located on the eastern side of the Jiamusi Block, which is separated by the Yuejinshan fault [56] or the Tongjiang-Toulin–Yingchun fault [50]. Moreover, geophysical data show that the tectonic boundary may be the Tongjiang–Baoqing–Dangbi region [57].

This complex is intruded by Cretaceous granites. On the basis of geology, specifically megaliths of a variety of rock types in a matrix of turbidite, this part of the NAC is referred to as the Tongjiang–Yuejinshan–Raohe accretionary complex in this study. The megalith types include peridotite, mid–ocean ridge basalt (MORB) or ocean island (OIB) basalt, deep–sea siliceous rock, seamount limestone (from seamounts), high–magnesium and Nb–enriched volcanic rock and arc igneous rock, all classically found in accretionary complexes. The overall trend of the Tongjiang–Yuejinshan–Raohe accretionary complex is north–south [12,14,18,20,30,32], and the NAC is referred to as the Tongjiang–Yuejinshan–Raohe accretionary complex in this study.

The Tongjiang accretionary complex is located in the northwestern part of the NAC belt and mainly outcrops in the Qindeli, Jiejinkou and Jiangbian regions (Figure 1c). The lithology of the block predominantly includes pyroxenite, basalt, siliceous rock, gabbro, andesite and rhyolite. A fault is apparent and cuts the block and matrices, with mylonitization having developed in some matrices. The zircon U–Pb ages of the blocks are as follows: basalt with an age ranging from 279–270 Ma [33,47], gabbro with an age of 288 ± 2 Ma [32], rhyolite with an age of ~279 Ma [32] and andesite with an age of ~174 Ma [18]. The mafic volcanic block exhibits an OIB affinity [32], the andesitic block indicates high–magnesium geochemical characteristics [18], and the gabbroic and rhyolitic rocks exhibit arc magmatic rock geochemical characteristics [32].

The Yuejinshan accretionary complex is located in the western part of the NAC and mainly outcrops in the Yuejinshan region in places such as Dongfanghong town and the 853 farm (Figure 1b). The lithology of the block predominantly includes ultramafic rocks (dunite, wehrlite and clinopyroxenite), basalt, greenschist, limestone and gabbro, and the formation age is mainly Permian and partly Late Triassic. The zircon U–Pb ages of the blocks are as follows: gabbro with ages ranging from 287–266 Ma [21,32,42,46,55] and basalt with ages of 277 ± 2 Ma [33] and 232 ± 5 Ma [55]. The matrix of the accretionary complex mainly includes felsic schist and some felsic mylonite. The youngest detrital zircon age of the felsic mylonites is 223 ± 7 Ma [55]. The blocks in the Yuejinshan accretionary complex exhibit a MORB or OIB affinity, such as the greenschist block with the geochemical characteristics of OIB basalt [55], mafic volcanic rock dominated by MORB and OIB basalt [32] and gabbroic block with arc magmatic rock geochemical characteristics [21].

The Raohe accretionary complex constitutes the main part of the NAC (Figure 1d) and lies roughly within 60 km of Raohe and abuts the Yuejinshan complex which lies to its southwest. The lithology of the block predominantly includes ultramafic igneous rock, gabbro, diabase, limestone, pillow basalt and siliceous rock with some manganese nodules [58]. Except for limestone containing Carboniferous–Permian fusulinids and corals [59], these blocks mainly formed in the Late Triassic and Early–Middle Jurassic. The zircon U–Pb ages of the Raohe accretionary complex are as follows: mafic intrusive rocks with ages of 219–214 Ma [14,20,51] and basalt with an age of 168–166 [14,20,53]. The Late Triassic–Early Jurassic radiolarian can be observed in the siliceous rock [60]. The blocks of the Early Jurassic volcanic rocks (basaltic andesite, dacite and rhyolite) in the Raohe accretionary complex have ages between 187 and 174 Ma [18]. The matrices of the Raohe accretionary complex mainly comprise clastic rocks such as sandstone, sandy mudstone and mudstone. The minimum peak age in the detrital zircon age spectra and youngest concordant age of the detrital zircons in the matrix correspond to the Middle–Late Jurassic (172–157 Ma) and early Early Cretaceous (140–133 Ma) [14,20,35,52]. The blocks of the Middle Jurassic basaltic volcanic rock in the Raohe accretionary complex exhibit an OIB affinity [14,17,53,54,61]. The Early Jurassic volcanic rocks that occur in the Dongshan, Haiyinshan and Qingshankou regions reveal Nb-enriched or arc geochemical characteristics [17].

3. Sampling and Petrography

A total of three clastic sedimentary rock samples of the Tongjiang accretionary complex (QDL–7–3, QDL–2–7 and QDL–1–2) were collected from outcrops (QDL–7, QDL–2 and

QDL–1) along a path from Qindeli farm to Linjiang town in the Tongjiang region, and the sampling locations are shown in Figure 1c. The three samples from the Tongjiang accretionary complex lie along a northeastern strike and 1–2 and 7–3 are about 25 km apart. From all three clastic sediments, detrital zircons were separated, and U–Pb dating and Hf isotopic analysis were conducted.

The sampling site of QDL–7–3 mainly exposes a matrix of fine silty mudstone and argillaceous siltstone, which is intruded by granodiorite porphyry (Figure 2a,b). Sample QDL–7–3 is fine silty mudstone with blastopelitic and micro–lepidoblastic texture and contains argillaceous minerals as the major components. The argillaceous compositions are tawny and crypto–crystal and partly underwent recrystallization, turning to a directional arrangement of scaly sericite (Figure 2c). Fine silty fragments constitute 20% of the framework, angular, subrounded and schistose monocrystallites and are equably distributed among the argillaceous compositions. The silty fragments predominantly include quartz with a few biotite, plagioclase, and argillaceous fragments, and the grain sizes range from 0.03–0.2 mm.

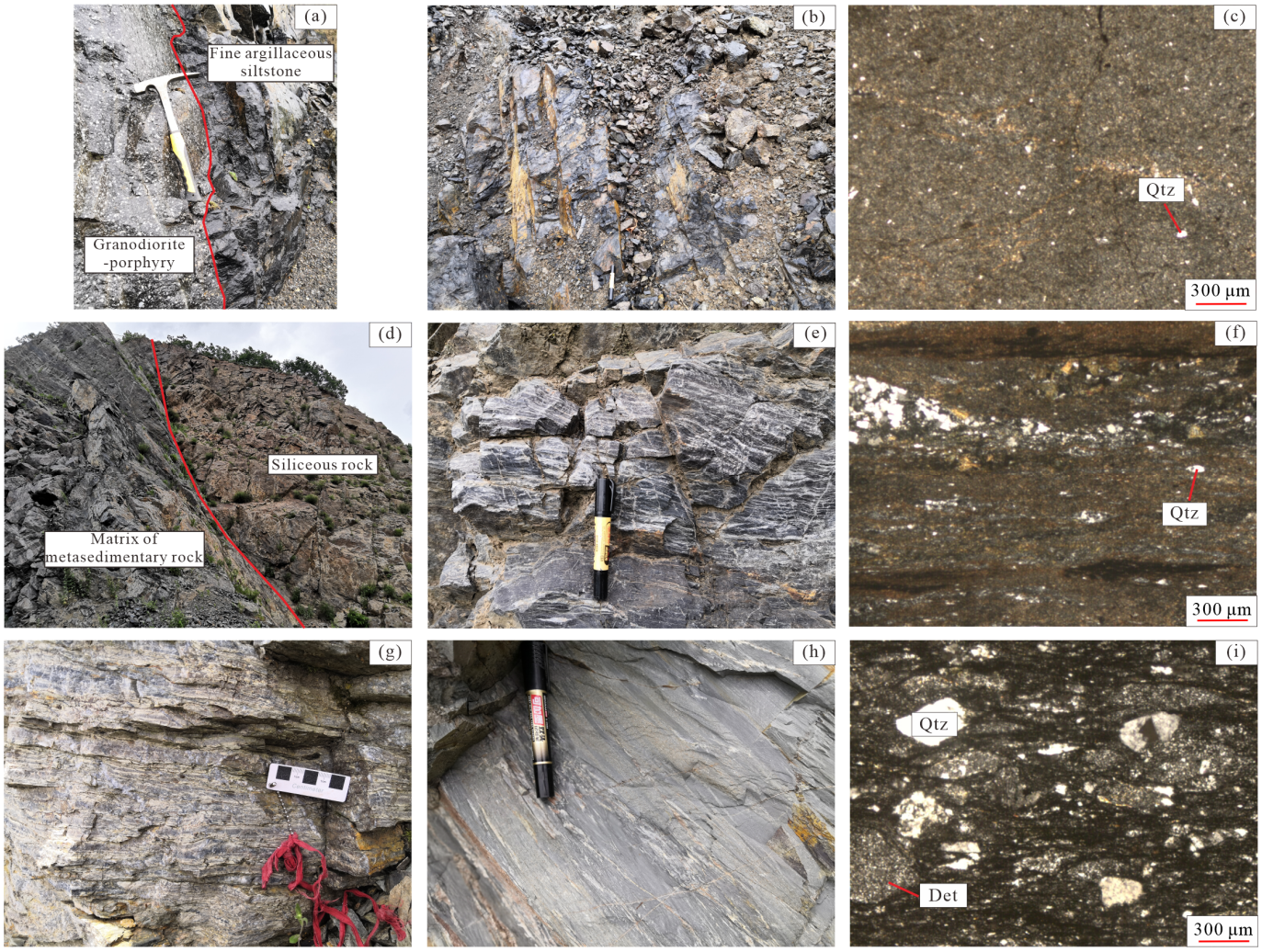


Figure 2. Photographs of field sampling sites and micrographs of the matrix in the Tongjiang accretionary complex. (**a**) Granodiorite porphyry intrudes into fine silty mudstone (QDL–7 sampling point); (**b**) Matrix composed of fine silty mudstone (QDL–7 sampling point); (**d**) Matrix composed of metamorphic sedimentary rocks and siliceous rock block with a fault contact (QDL–2 sampling point); (**e**) Matrix composed of phyllonite (QDL–2 sampling point); (**g**) Siliceous rock block (QDL–1 sampling point); (**h**) Matrix composed of mylonitizated fine argillaceous siltstone (QDL–1 sampling

point); (**c**,**f**,**i**) Fine sand silty mudstone respectively (QDL–7–3), phyllonite (QDL–2–7), and mylonitizated fine argillaceous siltstone (QDL–1–2) micrographs of the sample. Abbreviations: Qtz = quartz, Det = cuttings.

The sampling site of QDL–2–7 mainly exposes the pyroxenite and siliceous rock blocks and the matrix of sandy mudstone and phyllonite. The block has a fault contact with the matrix (Figure 2d,e). Sample QDL–2–7 is phyllonite, with a grain size generally smaller than 0.1 mm, and it exhibits a micro–lepidoblastic texture and schistose structure. This sample is characterized by dynamic recrystallization. The neogenic minerals are dominated by biotite, chlorite and hornblende, and the biotite is foliated. Felsic minerals are distributed in the biotite layer, with augen, lentoid and long ribbon shapes. Hornblende and chlorite are mainly distributed in the felsic aggregates. Biotite accounts for 45%, dynamically recrystallized felsic minerals account for 40%, and chlorite accounts for 10% of the total framework (Figure 2f).

The sampling site of QDL–1–2 mainly exposes andesite and siliceous rock blocks and a matrix of argillaceous siltstone and phyllonite. The block has a fault contact with the matrix (Figure 2g,h). Sample QDL–1–2 is fine argillaceous siltstone and has blasto–clastic and micro–lepidoblastic textures. The clastic components are predominantly composed of quartz, plagioclase, lithic fragments and white mica in a directional arrangement with grain sizes of 0.003–1 mm (a few are 3 mm in size). Quartz (15%) has wavy and banded extinction, with angular to subangular shapes. Plagioclase (5%) exhibits polysynthetic twinning and slight sericitization, with angular and subangular–to–subhedral tabular shapes. The lithic fragments (20%) are dominated by felsic lava with a small amount of mudstone and exhibit augen and long ribbon shapes. The interstitial cryptocrystalline material and recrystallized neogenic minerals are dominated by biotite, chlorite and sericite, with a micro–lepidoblastic texture, and are directionally distributed around the fragments (Figure 2i).

4. Analytical Methods

4.1. Zircon U–Pb Dating

Zircon grains were separated using conventional heavy–liquid and magnetic techniques and then picked by hand picking under a binocular microscope. Zircon grains for each sample were mounted in epoxy resin, and the centers of the grains were polished. All zircon grains were photographed in transmitted light, reflected light and cathodoluminescence (CL) to identify morphology and internal structures to select suitable crystals and analytical points. Zircon U–Pb isotopic analyses were synchronously performed on a GeolasPro laser ablation system attached to an Agilent 7900 inductively coupled plasma block spectrometry (ICP–MS) instrument at Wuhan SampleSolution Analytical Technology Co., Ltd. (Wuhan, China). The spot size of the laser was set to 24 μm, and helium was used as a carrier gas to transfer ablated materials. The analytical technique was the same as that described by Zong et al. (2017) [62]. The U–Pb date was normalized using zircon 91500 as external standard, and GJ–1 was used as monitor standard. Each analysis incorporated a background acquisition of approximately 20–30 s followed by 50 s of data acquisition. ICPMSDataCal software was used to perform off-line selection [63,64]. Weighted average age calculation and probability density plotting were conducted using Isoplot/Ex_ver3 software [65]. The method for calculating discordance for U–Pb data is (^{207}Pb/^{235}U age)/(^{206}Pb/^{238}U age)×100. ^{204}Pb is used to make common Pb correction. Zircon ages were taken as ^{207}Pb/^{206}Pb ages for grains older than 1000 Ma and ^{206}Pb/^{238}U ages for grains younger than 1000 Ma. The results are presented in Supplementary Table S1 and the uncertainties are 1σ.

4.2. Zircon Hf Isotopes

In situ Lu–Hf isotopic analyses were performed on the Geolas HD excimer ArF laser–ablation system attached to a Neptune Plus multi–collector inductively coupled plasma block spectrometer (MC–ICP–MS) at Wuhan SampleSolution Analytical Technology Co., Ltd. A spot size of 44 μm was used, and helium was used as a carrier gas to transfer

ablated materials. The analytical technique was the same as that of Hu et al. (2012) [66]. Zircon Hf isotope interference correction was the same as that described by Blichert–Toft et al. (1997) [67] and Fisher et al. (2014) [68]. The data between reference material calculations were mass bias–corrected using ICPMSDataCal [64]. The results are presented in Supplementary Table S2.

5. Results

5.1. Zircon U–Pb Dating

The zircon grains in sample QDL–7–3 are primarily granular with some short prismatic anhedral–subhedral crystals. They have lengths ranging from 45 to 100 μm and length–to–width ratios between 1:1 and 2:1. Zircon grains show well–developed oscillatory zoning (Figure 3a) and high Th/U ratios (0.15–1.48), indicating a typical magmatic origin. In total, 56 detrital zircon analyses were performed, and 55 single zircon grains with a concordance exceeding 90% were selected for final interpretation. The concordant ages range from 247–1789 Ma, and the age spectrum yields four main peak ages of 265 Ma, 341 Ma, 401 Ma and 474 Ma, and older concordant ages are 773 ± 9 Ma, 983 ± 10 Ma, 1350 ± 57 Ma and 1789 ± 45 Ma. Thirty–seven detrital zircons define a weighted mean age of 261.4 ± 2.9 Ma (MSWD = 5.5), and the youngest grain yields an age of 247 ± 3 Ma (Figure 4a,b).

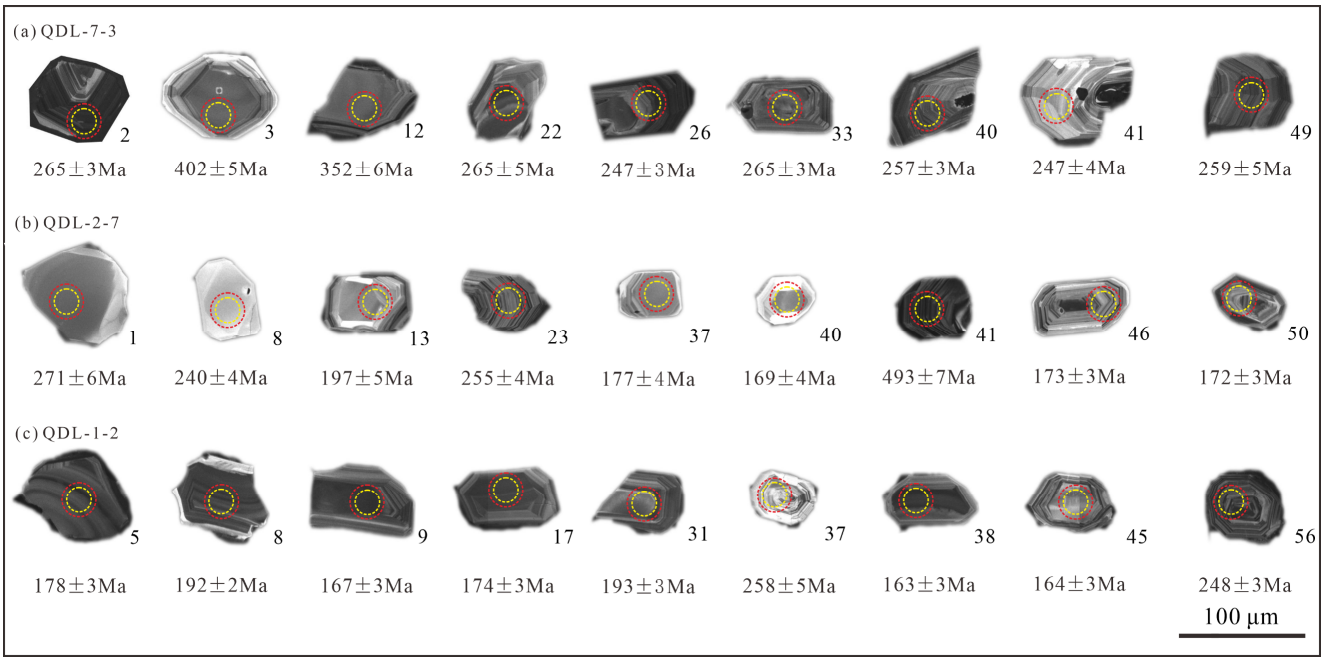


Figure 3. Representative CL images of detrital zircons from samples QDL–7–3, QDL–2–7 and QDL–1–2 with laser spots. The yellow circles represent the dating spots for U–Pb analyses and red circles represent the locations of in situ Hf isotope analyses. The uncertainties are 1σ.

The zircon grains in sample QDL–2–7 are primarily granular with some short prismatic anhedral–subhedral crystals. They have lengths ranging from 50 to 90 μm and length–to–width ratios between 1:1 and 2:1. Zircon grains show well–developed oscillatory zoning (Figure 3b) and high Th/U ratios of 0.13–1.05 (some grains have ratios of 0.02–0.09), indicating a typical magmatic origin. In total, 57 detrital zircon analyses were performed, and 54 single zircon grains with a concordance exceeding 90% were selected for final interpretation. The concordant ages range from 172–1743 Ma and the age spectrum yields five main peak ages of 172 Ma, 251 Ma, 500 Ma, 880 Ma and 954 Ma, and older concordant ages are 759 ± 9 Ma, 1231 ± 57 Ma, 1228 ± 69 Ma, 1377 ± 52 Ma, 1559 ± 72 Ma and 1743 ± 65 Ma. Fifteen detrital zircons define a weighted mean age of 502.5 ± 5.9 Ma (NSWD = 2.5), six de-

trital zircons define a weighted mean age of 175.2 ± 4.9 Ma (NSWD = 2.2), and the youngest grain yields an age of 169 ± 4 Ma (Figure 4c,d).

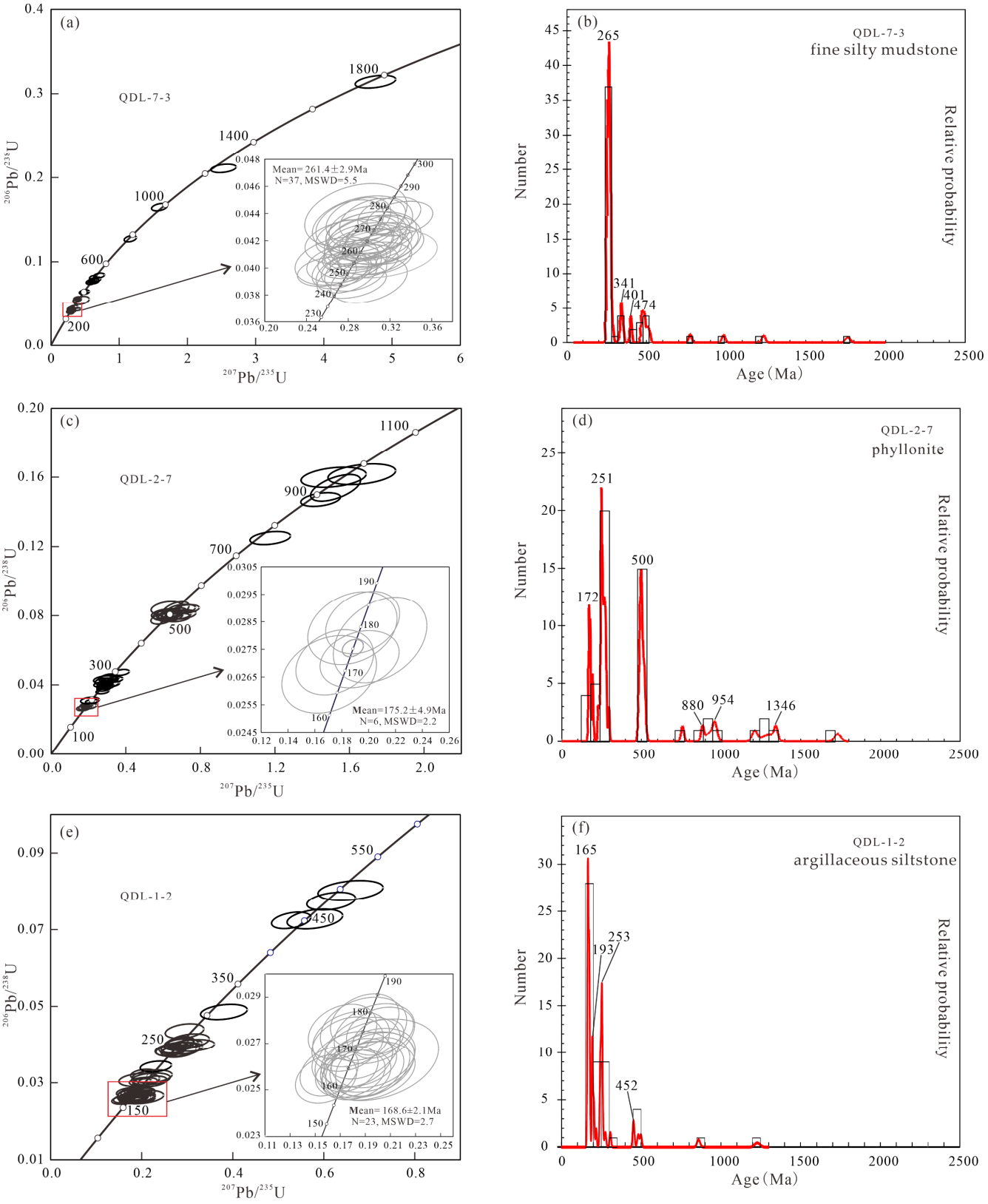


Figure 4. U–Pb concordia diagrams (**a**,**c**,**e**) and normalized probability distribution (**b**,**d**,**f**) of detrital zircon ages from samples QDL–7–3, QDL–2–7 and QDL–1–2.

The zircon grains in sample QDL–1–2 are primarily granular or short prismatic anhedral–subhedral crystals. They have lengths ranging from 50 to 100 μm and length–to–width ratios between 1:1 and 2:1. Zircon grains show well-developed oscillatory zoning (Figure 3c) and high Th/U ratios of 0.25–1.87 (one grain has a ratio of 0.04), indicating a typical magmatic origin. In total, 58 detrital zircon analyses were performed, and 53 single zircon grains with a concordance exceeding 90% were selected for final interpretation. The concordant ages range from 162–1209 Ma and the age spectrum yields four main peak ages of 165 Ma, 193 Ma, 253 Ma and 452 Ma, and older concordant ages are 306 ± 5 Ma, 481 ± 6 Ma, 498 ± 6 Ma, 860 ± 10 Ma and 1209 ± 88 Ma. Fourteen detrital zircons define a weighted mean age of 249.7 ± 3.1 Ma (NSWD = 2.3), seven detrital zircons define a weighted mean age of 195.4 ± 4.5 Ma (NSWD = 2.1), and the youngest grain yields an age of 162 ± 3 Ma (Figure 4e,f).

5.2. Zircon Hf Isotopes

The zircon grains in the Early–Middle Jurassic (163–197 Ma) age population from three samples have $^{176}Hf/^{177}Hf$ ratios ranging from 0.281956 to 0.282897, mainly positive $\varepsilon_{Hf}(t)$ values ranging from −25.4 to +7.9, and two–stage model (T_{DM2}) ages ranging from 717 to 2814 Ma. The zircon grains in the Early–Middle Triassic (240–251 Ma) age population have $^{176}Hf/^{177}Hf$ ratios ranging from 0.282582 to 0.282661, mainly positive $\varepsilon_{Hf}(t)$ values ranging from −1.4 to +1.3, and T_{DM2} ages ranging from 1199 to 1365 Ma. The zircon grains in the Middle–Late Permian (255–271 Ma) age population have $^{176}Hf/^{177}Hf$ ratios ranging from 0.282504 to 0.282938, mainly positive $\varepsilon_{Hf}(t)$ values ranging from −4 to +11.7, and T_{DM2} ages ranging from 549 to 1535 Ma. The zircon grains in the Devonian–Carboniferous (352–402 Ma) age population have $^{176}Hf/^{177}Hf$ ratios ranging from 0.282273 to 0.282776, mainly positive $\varepsilon_{Hf}(t)$ values ranging from −9.2 to +7.5, and T_{DM2} ages ranging from 876 to 1976 Ma. The zircon grains in the Late Cambrian–Early Ordovician (473–505 Ma) age population have $^{176}Hf/^{177}Hf$ ratios ranging from 0.282358 to 0.282566, mainly positive $\varepsilon_{Hf}(t)$ values ranging from −4.1 to +2.9, and T_{DM2} ages ranging from 1265 to 1730 Ma. The zircon grains in the Mesoproterozoic and Neoproterozoic (860–1377 Ma) age populations have $^{176}Hf/^{177}Hf$ ratios ranging from 0.282071 to 0.282363, mainly positive $\varepsilon_{Hf}(t)$ values ranging from −0.8 to +12.2, and T_{DM2} ages ranging from 1262 to 1902 Ma.

6. Discussion

6.1. Depositional Age of the Matrix of the Tongjiang Accretionary Complex

The lithology of the matrix of the Tongjiang accretionary complex is primarily composed of fine argillaceous siltstone, argillaceous siltstone, pebbly sandy mudstone, fine silty mudstone, silty mudstone, mudstone and phyllonite with partially developed mylonitization in the matrix. In this study, we use the zircon U–Pb dating results of samples QDL–7–3, QDL–2–7 and QDL–1–2, which were collected from west to east in the Tongjiang accretionary complex, to constrain the formation age of the matrix. The age of detrital zircons can effectively constrain the stratum depositional age, and the youngest U–Pb concordant age of detrital zircon represents the maximum depositional age [69–71]. The maximum depositional age must be younger than the age of the youngest detrital zircon [72]. We combined the youngest detrital zircon age and the youngest weighted average age to constrain the lower limit of the formation age of the matrix.

The detrital zircon ages of sample QDL–7–3 are dispersive and continuous. Thirty–seven detrital zircons define the youngest weighted mean age of 261.4 ± 2.9 Ma, and the two youngest grains yield ages of 247 ± 3 Ma and 247 ± 4 Ma, indicating that the lower limit of the formation age ranges from 261–247 Ma. Six detrital zircons in sample QDL–2–7 define the youngest weighted mean age of 175.2 ± 4.9 Ma, and the youngest grain yields an age of 169 ± 4 Ma, indicating that the lower limit of the formation age is 175 Ma. Twenty–three detrital zircons in sample QDL-1-2 define the youngest weighted mean age of 168.6 ± 2.1 Ma, and the youngest grain yields an age of 162 ± 3 Ma, indicating that the lower limit of the formation age is 169 Ma.

We speculate that the formation age of the matrix of the Tongjiang accretionary complex may be the Late Permian–Early Triassic and Middle Jurassic, and the formation age of the matrix of clastic rocks exhibits a younging trend from west to east.

6.2. Provenance of Detrital Zircons in the Matrix of the Tongjiang Accretionary Complex

Zircon can maintain a stable U–Pb isotope system in geological processes [73], and the provenance of the sediment can be effectively constrained by comparing the detrital zircon age composition of the stratum with the geochronology data in the region that experienced relatively frequent magmatic activities [74]. The zircon grains in the matrix of the Tongjiang accretionary complex show well–developed oscillatory zoning with high Th/U ratios (mostly >0.2), indicating a typical magmatic origin. Thus, the age information of these detrital zircons could correctly constrain the provenance of sediment in the matrix. The age distributions of samples QDL–7–3, QDL–2–7 and QDL–1–2 reveal highly similar age peaks, including the Middle Jurassic (165 Ma and 172 Ma) and the Middle–Late Permian (253 Ma and 265 Ma), which indicates that these samples have partly the same source ages.

The Jurassic detrital zircons are mainly Early–Middle Jurassic (201–162 Ma). The samples QDL–1–2 and QDL–2–7 define weighted mean ages of 168.6 ± 2.1 Ma, 175.2 ± 4.9 Ma and 195.4 ± 4.5 Ma, and these ages are temporally associated with the formation age of the Early Jurassic igneous blocks and Middle Jurassic oceanic island igneous blocks in the NAC belt (Figure 5a,c) [18,75]. During the migration and subduction process, the intra–oceanic island arc and oceanic island suffered continuous subduction and accretion and were eroded to become sediment sources. An oceanic island is likely the main source of the 160–200 Ma detrital zircons [35]. Examples include the Early Jurassic (187–174 Ma) volcanic blocks in the Tongjiang and Raohe accretionary complexes [18] and the Middle Jurassic (168–166 Ma) pillow basalt blocks in the Dadai region [14,20,53]. The zircons in this age population have positive $\varepsilon_{Hf}(t)$ values with Neoproterozoic T_{DM2} ages, which are similar to those of the zircon Hf isotopic compositions of the Early Jurassic volcanic blocks in the Tongjiang and Raohe accretionary complexes [18]. In addition, the Early Jurassic igneous rocks in the Xingkai block may provide material sources [76]. A Middle Jurassic detrital zircon sample has a $\varepsilon_{Hf}(t)$ value of −25.4, which is same as that of a zircon sample's $\varepsilon_{Hf}(t)$ value of −22.9 from the Jiamusi Block. Such strongly negative values indicate Archean sources have provided zircons to the melange. The latter is related to the assimilation of the Precambrian ancient crust; both contain this ancient component.

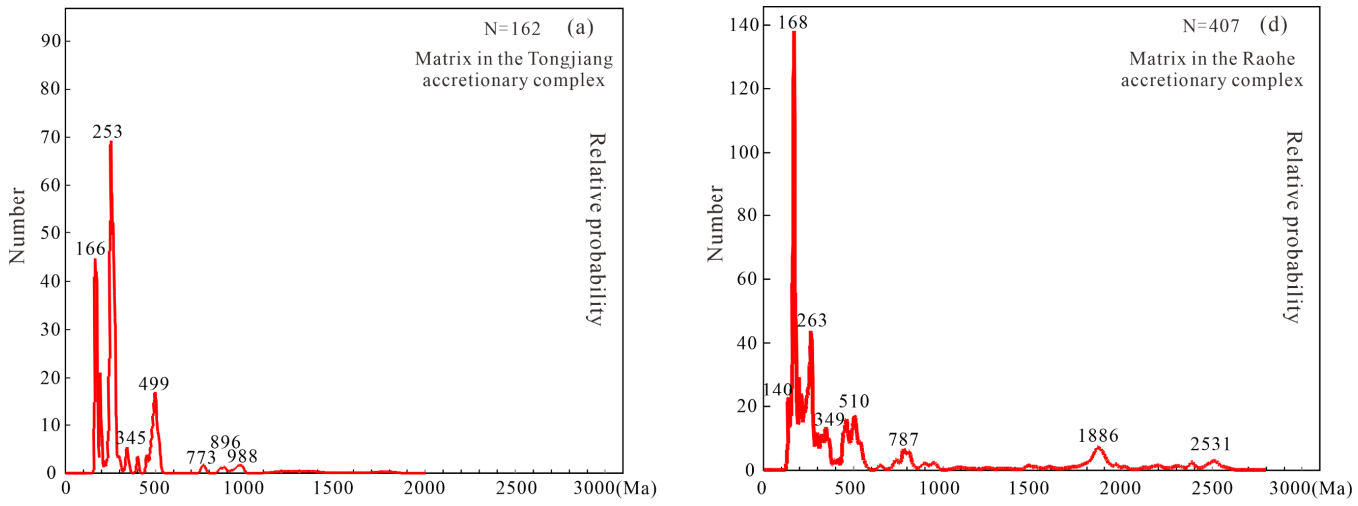


Figure 5. *Cont.*

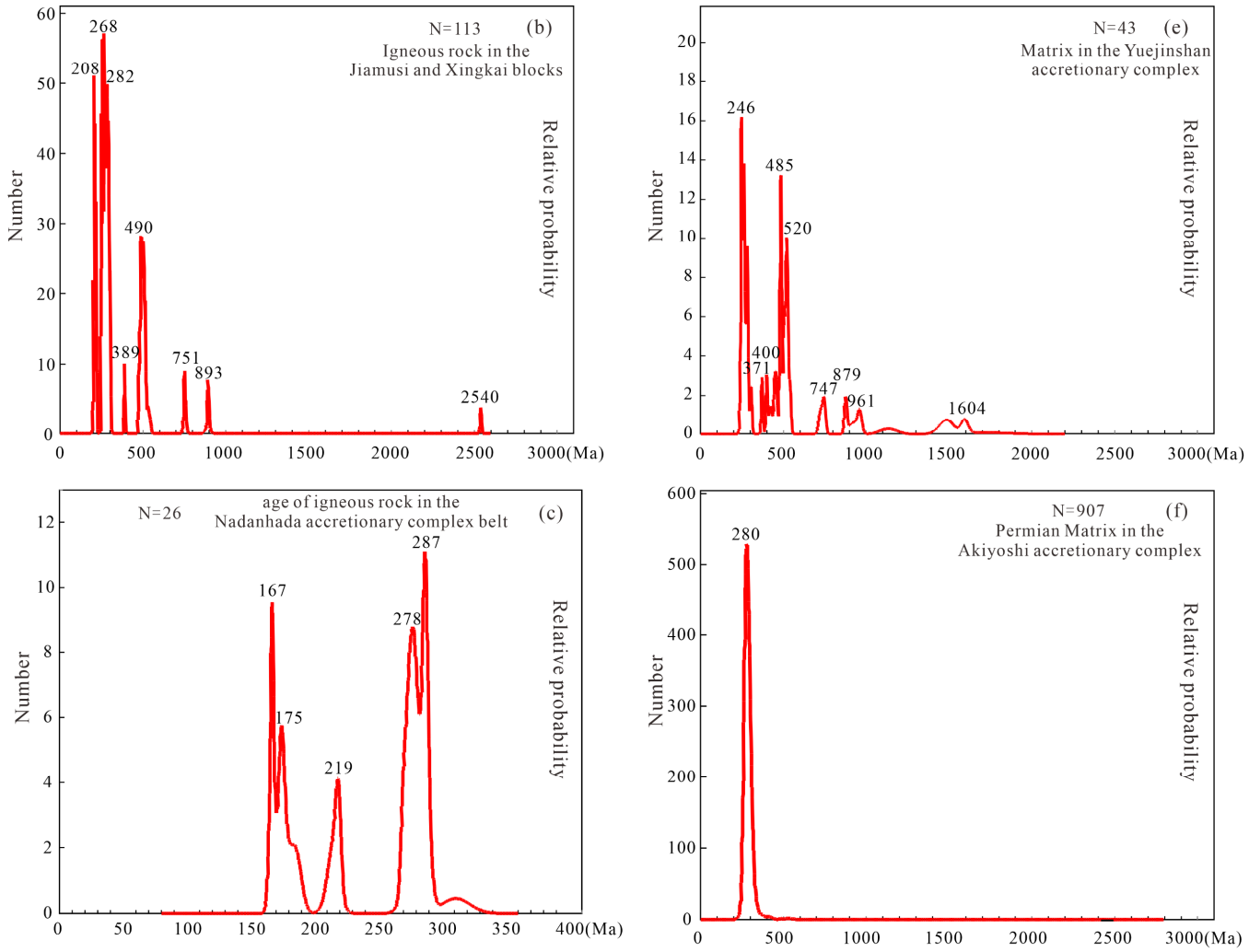


Figure 5. (**a**) The distribution of detrital zircon ages from matrix in the Tongjiang accretionary complex; (**b**) Igneous rock in the Jiamusi and Xingkai blocks [22,32,40,46,77–88]; (**c**) Ages of igneous rock in the NAC belt [14,17,20,32,46,47,51]; (**d**) Matrix in the Raohe accretionary complex [14,20,35,52]; (**e**) Matrix in the Yuejinshan accretionary complex [55]; (**f**) Permian Matrix in the Akiyoshi Belt [89].

The Triassic detrital zircons are mainly Triassic (252–204 Ma). The youngest dominant zircon population in QDL–1–2 defines a weighted mean age of 249.7 ± 3.1 Ma, and this age is temporally associated with the Early–Middle Triassic granites in the Jiamusi and Xingkai blocks. Examples include the Early–Middle Triassic granites (250–246 Ma) in the Jiamusi Block [22] and the granodiorite (~249 Ma) in the Xingkai Block [77]. Zircons in this age population have $\varepsilon_{Hf}(t)$ values ranging from −1.4 to +1.3 with Mesoproterozoic T_{DM2} ages, which are similar to those of the zircon Hf isotopic compositions of the Early–Middle Triassic intrusive rocks in the Jiamusi and Xingkai blocks (Figure 6) [22].

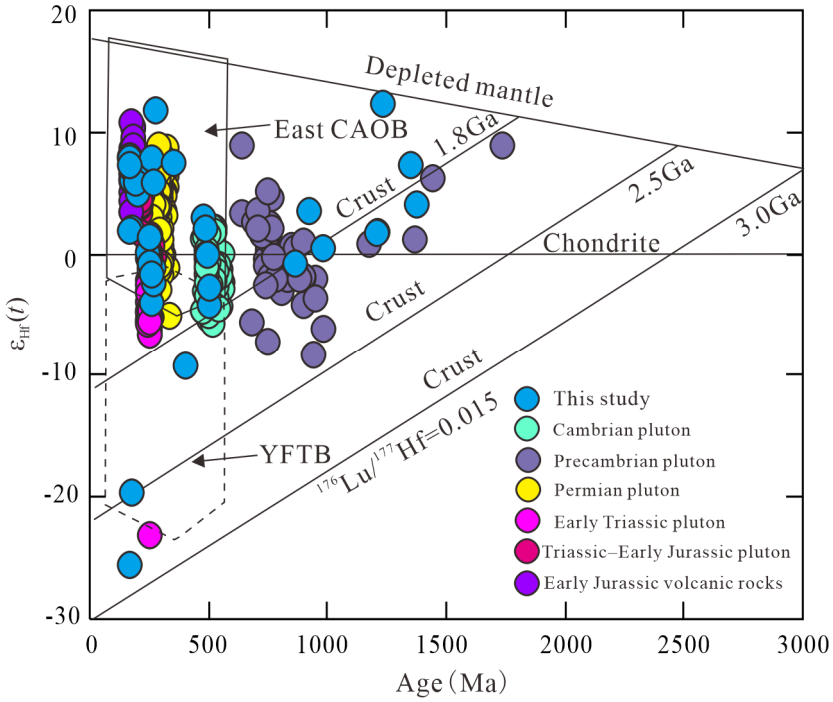


Figure 6. ε_{Hf}(t) versus U–Pb ages of zircons. CAOB—the Central Asian Orogenic Belt, YFTB—the Yanshan Fold and Thrust Belt [90]. Previous data: Cambrian pluton in the Jiamusi Block [83]; Precambrian pluton in the Jiamusi Block [84]; Permian pluton in the Jiamusi and Xingkai blocks [32,80]; Triassic–Early Jurassic pluton in the Jiamusi and Xingkai blocks [22,77]; Early Jurassic volcanic rocks in the NAC belt [18].

Permian (297–253 Ma) detrital zircons are the most common in the analyzed samples. Sample QDL–7–3 defines a weighted mean age of 261.4 ± 2.9 Ma, and this age is temporally associated with the Permian igneous blocks in the Yuejinshan and Tongjiang accretionary complexes and Permian igneous rocks in the Jiamusi and Xingkai blocks (Figure 5a–c). Examples include granites with ages of 294~254 Ma in the Jiamusi Block [32,46,78–81] and volcanic rocks with ages of 293~263 Ma in the eastern region [32,38,39], granites with ages of 296~257 Ma in the Xingkai Block [80] and the basalt, gabbro and rhyolite blocks in the Yuejinshan and Tongjiang accretionary complexes [21,32,42,46,47,55]. Zircons in this age population have ε_{Hf}(t) values ranging from −4 to +11.7 with Mesoproterozoic and Neoproterozoic T_{DM2} ages, which are similar to those of the zircon Hf isotopic compositions of the Permian granites in the Jiamusi and Xingkai blocks (Figure 6) [32,80]. Devonian and Carboniferous (402–306 Ma) detrital zircons are minor components that correspond to the Devonian and Carboniferous volcanic–sedimentary sequences in the eastern margin of the Jiamusi Block [91], such as the Laotudingzi Formation rhyolite dated at 392–388 Ma [82].

Cambrian–Ordovician (523–451 Ma) detrital zircons are temporally associated with the Cambrian–Ordovician granites in the Jiamusi and Xingkai blocks [83–85] (Figure 5a,b). Precambrian detrital zircons are a minor component and are mainly Mesoproterozoic and Neoproterozoic in age (1789–759 Ma). This age is temporally associated with the Mesoproterozoic and Neoproterozoic igneous rocks and metamorphic strata in the Jiamusi Block. Examples include the granitic gneiss (898–751 Ma) in the Jiamusi Block [84,86] and the Paleoproterozoic and Mesoproterozoic detrital zircon age peaks in the Precambrian metamorphic stratum [92].

Therefore, we suggest that the detrital zircons in the matrix of the Tongjiang accretionary complex may be mainly derived from blocks in the NAC belt and the Jiamusi and Xingkai blocks. The source rocks are the Precambrian terranes and Paleozoic–Mesozoic igneous rocks in the Jiamusi and Xingkai blocks and the Permian and Early–Middle Jurassic igneous blocks in the NAC belt (Figure 5a–c). The detrital zircon age spectra of the matrix

of the Tongjiang, Raohe and Yuejinshan accretionary complexes have some similar age peaks, such as the Proterozoic, Cambrian and Permian age peaks, which indicates that these matrices share some of the same source rocks (Figure 5a,d,e). The detrital zircons in the matrices of the Raohe accretionary complex may be mainly derived from the neighboring Jiamusi and Xingkai blocks, and the Precambrian detrital zircons may be sourced from the Precambrian basement of NE China [14].

6.3. Implications for the Westward Subduction and Accretion Process of the Paleo–Pacific Ocean

The most direct material record of the Paleo–Pacific tectonic regime in NE China is the NAC belt, which is related to subduction. Most studies in recent years have suggested that the Raohe accretionary complex in this belt was the product of Paleo–Pacific subduction and accretion [12,15,34–36]. However, the mechanism of subduction of the Yuejinshan accretionary complex has different interpretations, and various opinions have been held about the Paleo–Pacific Ocean [12,20], Paleo–Asian Ocean [15] or Panthalassa [30,34,53]. Moreover, combined with the different degrees of extent and metamorphism between the Yuejinshan and Raohe accretionary complexes and the Yuejinshan accretionary complex being lodged between the two plates based on geophysical characteristics, some scholars have proposed that the Yuejinshan accretionary complex is the product of subduction of the Paleo–Asian Ocean [15,31]. However, the electrical architectural feature of the deep crust indicates that it is an accretionary complex [93]. Based on the initial Late Triassic–Early Jurassic subduction age of the Paleo–Pacific Plate, others have suggested that the Yuejinshan accretionary complex is the product of the Panthalassa [30]. According to the results of previous studies of the formation age of the Mesozoic igneous rock and accretionary complex in the NAC and the Permian arc igneous rock in the Jiamusu Block, different arguments have been put forward to constrain the initial subduction age of the Paleo–Pacific to the Early Jurassic [15–19], Late Triassic [11,20,34] or Permian [21,22,45]. Three observations leading to the conclusion that the subduction direction was toward the west are as follows: (1) The Tongjiang accretionary complex matrix is dated to be Late Permian–Early Triassic and Middle Jurassic; (2) the detritus is likely mainly derived from the neighboring Jiamusi and Xingkai blocks to the west on the continental side of the accretionary complexes; and (3) a west–to–east younging direction for formation of the complex can be assumed based on our data (Figure 7). In combination with the research results of the Yuejinshan and Raohe accretionary complexes, we further determine that the NAC is the product of the subduction and accretion of the Paleo–Pacific Plate, and we offer a model of the subduction and accretion processes during the Late Paleozoic–Mesozoic.

The initial arc material is an important petrologic distinguishing basis for the initial subduction of the ocean basin, and mainly refers to the frontal arc basalt, boninite/high–magnesium andesite, adakite and Nb–enriched arc igneous rock in the subduction zone's island frontal arc region [94–98]. The frontal arc basalt is the lava formed in the first eruption at the initial stage of the intra-oceanic subduction [94,95,98].

The initial Permian arc igneous associations are exposed in the Yuejinshan accretionary complex. For instance, the Dongfanghong block of the Permian metabasalt (277 ± 2 Ma) [33] with a normal mid–ocean ridge basalt (N-MORB) affinity [20] has double the geochemical characteristics of the mid–oceanic ridge and island arc, similar to the frontal arc basalt (FAB) [99]. The Hamatong block of the Permian metabasalt (274 ± 3 Ma) has an enriched mid–ocean ridge basalt (E-MORB) affinity [47], which is similar to the geochemical characteristics of the Nb–enriched arc basalt and basaltic andesite (NEAB) [99]. The eastern Paleo–Asian Ocean closed during the Middle Triassic [9,13] or Early–Middle Triassic [34,100]. The block of the Late Triassic basalt (232 ± 5 Ma) with an E–MORB affinity has been reported in the Yuejinshan accretionary complex [55], which indicates that the Paleo–ocean recorded by this accretionary complex still existed during the Late Triassic and was not the product of Paleo–Asian Ocean subduction during the Permian.

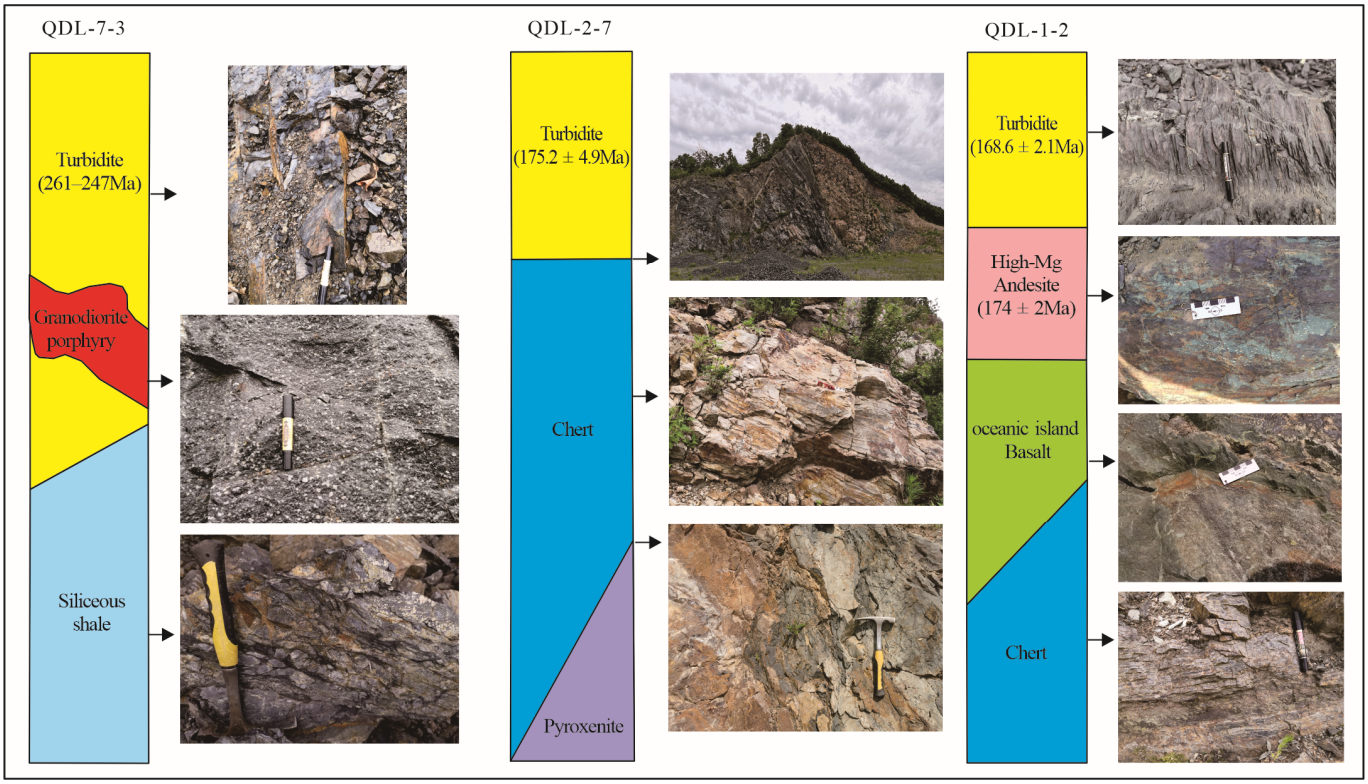


Figure 7. Simplified map of the oceanic plate stratigraphy of the Tongjiang AC (outcrop of this study). The andesite ages were obtained from [18].

The NAC belt and the accretionary complex belts in the Russian Far East and Japanese islands related to the westward subduction of the Paleo–Pacific Plate are distributed in eastern Eurasia [14], and a small number of Permian accretionary complexes are distributed in the Russian Far East and Japan [101]. The Permian–Early Triassic (299–245 Ma) arc magmatic rocks in the eastern Jiamusi Block [22], the Permian arc igneous rocks in the Jiamusi Block [99], the Xingkaihu granites (~250 Ma) in the Xingkai Block [77] and the gabbro blocks in the Yuejinshan accretionary complex [21] are interpreted as the product of the subduction of the Paleo–Pacific Plate. In addition, the large region of Late Permian—Triassic island arc magmatic rocks exposed in the southeastern South China Block is also considered to have formed during westward subduction of the Paleo–Pacific Plate [102]. It should be noted that the Permian detrital zircons from the Akiyoshi accretionary complex in southwestern Japan were derived from the Permian volcanic arc related to the subduction of the Paleo–Pacific Plate [89], which is similar in age to that of the youngest detrital zircon (261.4 ± 2.9 Ma) and the provenance of sample QDL–7–3 (Figure 5a,f). Before the Miocene opening of the Japan Sea, the Tongjiang and Yuejinshan accretionary complexes and the Permian accretionary complexes in the Russian Far East and Japan may be Permian accretionary complex belts, which are the product of the subduction and accretion of the Paleo–Pacific Ocean.

The NAC belt not only constrains the initial subduction age of the Paleo–Pacific Plate but also records the subduction and accretion process of the Paleo–Pacific Plate. The following two models document the aforementioned subduction and accretion process: (1) The Paleo–Pacific Plate began and continued to subduct in the Late Triassic, and the Yuejinshan accretionary complex was formed in the Late Triassic to Early Jurassic in the western part of the NAC. The Raohe accretionary complex was formed in the Middle Jurassic to Early Cretaceous in the eastern part of the NAC, which has a younging trend from west to east [14,20]. (2) The Paleo–Pacific Plate began to subduct in the Early Jurassic, which resulted in the formation of the Raohe accretionary complex and was in place in

the Early Cretaceous [15]. In order to reveal the subduction and accretion process of the Paleo–Pacific Ocean, we combine the lower limit of the depositional age of the matrix of the Late Permian to Early Triassic and the Middle Jurassic for the Tongjiang accretionary complex, the Late Triassic for the Yuejinshan accretionary complex, the Middle Jurassic–Early Cretaceous for the Raohe accretionary complex and chronological data of the blocks in the NAC belt. We preliminarily consider that the NAC belt is composed of Late Permian–Triassic, Jurassic and Early Cretaceous accretionary complexes from west to east. These accretionary complexes at different stages could correspond to accretionary complexes exposed in the Russian Far East and Japan [101,103,104].

Based on the Permian initial subduction age of the Paleo–Pacific Plate and the Late Permian–Triassic, Jurassic and Early Cretaceous accretionary complexes are distributed from west to east in the NAC belt with a younging trend of the accretion materials from west to east. We preliminarily establish a westward subduction and accretion process of the Paleo–Pacific Plate in the Wandashan region during the Permian to Early Cretaceous (Figure 8).

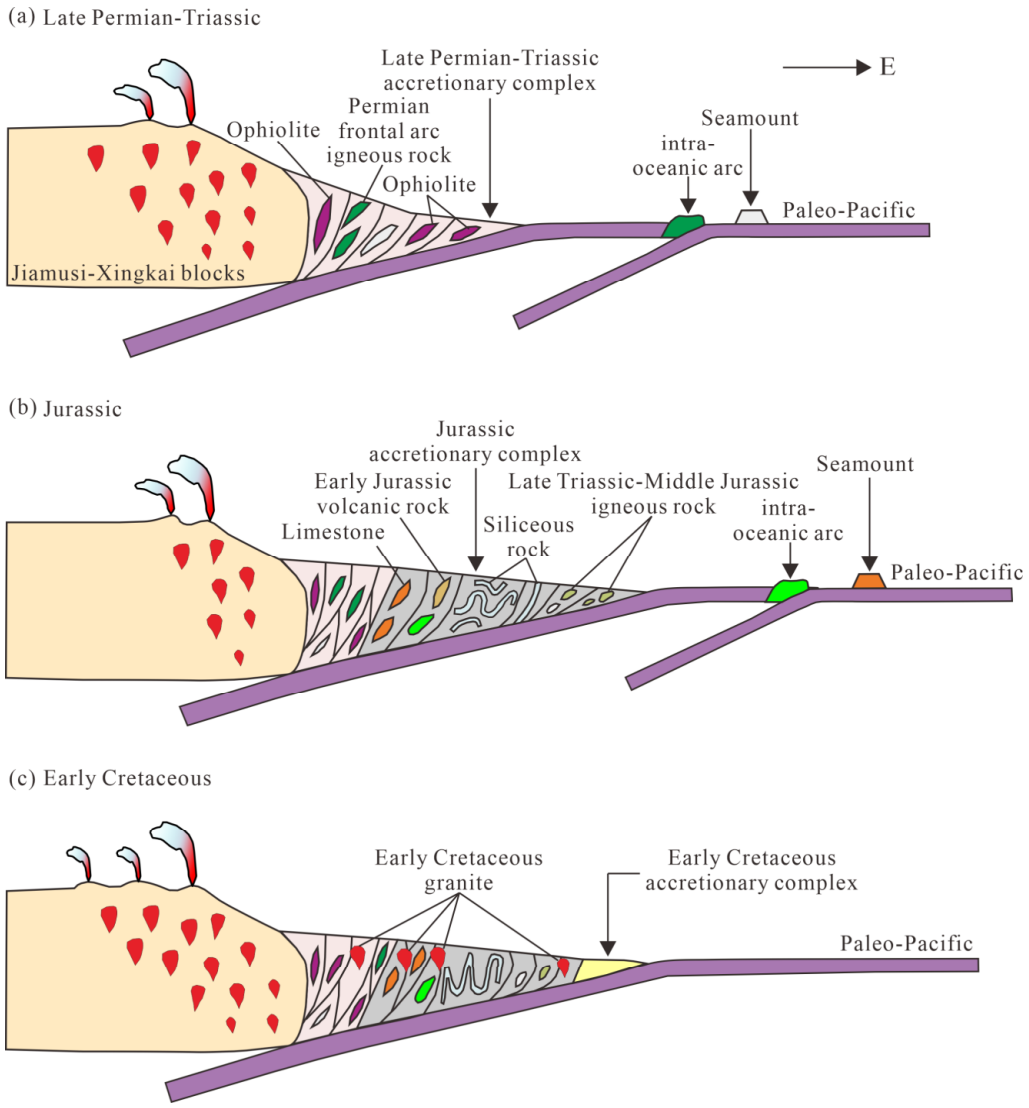


Figure 8. Schematic diagram depicting the subduction and accretion process of the Paleo–Pacific Plate. (**a**) Late-Permian Triassic, (**b**) Jurassic, (**c**) Early Cretaceous.

The Paleo–Pacific Plate began to subduct westward in the Permian. The initial arc igneous assemblage of the frontal arc basalt and Nb–enriched arc basalt is related to the

Permian initial subduction. The Late Permian–Triassic accretionary complex was in place in the eastern Jiamusi Block in the late Late Triassic and was mainly derived from the terranes in the Jiamusi and Xingkai blocks (Figure 8a). Based on the youngest detrital zircon weighted mean age of 261.4 ± 2.9 Ma, the youngest detrital zircon age of ~247 Ma of fine silty mudstone in the Tongjiang region and the youngest weighted mean age of 223 ± 7 Ma of the matrix of felsic mylonite in the Yuejinshan region [55], the accretionary age of this accretionary complex is the Late Permian–Triassic. The block is dominated by ultramafic rock, greenschist, limestone and basalt as well as gabbro of Permian age [32,33,47].

The Paleo–Pacific Plate began to subduct in the Jurassic and Early Jurassic intra-oceanic subduction, resulting in the formation of high–magnesium andesite and Nb–enriched basaltic andesite and is characterized by widely developed ocean island igneous rocks. The Late Jurassic accretionary complex experienced accretion in the Late Permian–Triassic accretionary complex, which was mainly derived from the terranes in the Jiamusi and Xingkai blocks and the Early–Middle Jurassic igneous blocks in the accretionary complex (Figure 8b). On the basis of the youngest detrital zircon weighted mean ages of 175.2 ± 4.9 Ma and 168.6 ± 2.1 Ma for samples QDL–2–7 and QDL–1–2, the youngest weighted mean ages of 167 ± 17 Ma and 167 ± 3 Ma for the Hongqiling matrix of sandstone [20] and Dadai matrix of silty mudstone [14], and the youngest weighted mean ages of 172 ± 4 Ma, 157 ± 3 Ma and 167 ± 1 Ma for the matrix of the Dalingqiao Formation sandstone in the Raohe region [35], the accretionary age of this accretionary complex is the Jurassic. The block is dominated by ultramafic rock, limestone, siliceous rock, Late Triassic gabbro and sillite [14,20,51], Early Jurassic volcanic rock [18] and Middle Jurassic pillow basalt [14,18,20,53].

The Paleo–Pacific Plate continued to subduct in the Early Cretaceous, and the Early Cretaceous accretionary complex experienced accretion in the Jurassic accretionary complex during the late Early Cretaceous (Figure 8c). On the basis of the youngest detrital zircon weighted mean ages of 137 ± 1 Ma [20] and 133 ± 4 Ma [14] from sandstone in eastern Dadai and 140 ± 2 Ma from sandstone in eastern Dadingzishan [52], the depositional age of this accretionary complex is the Early Cretaceous.

7. Conclusions

Based on the detrital zircon U–Pb ages and Hf isotopic data presented in this study, we draw the following conclusions:

1. The lower limit of the depositional age of the matrix of the fine silty mudstone, phyllonite and mylonitized fine argillaceous siltstone in the Tongjiang accretionary complex may be 261–247 Ma, 175 Ma and 168 Ma, respectively, with a younging trend from west to east. Provenance analysis suggested that the detrital zircons may be mainly derived from blocks in the NAC belt and the Jiamusi and Xingkai blocks;
2. Combining the lower limit of the depositional age of the matrix in the Yuejinshan and Raohe accretionary complexes and chronological data of the blocks in the NAC belt, we propose that the NAC may be mainly composed of the Late Permian Triassic, Jurassic and Early Cretaceous accretionary complexes from west to east and is the material record of the subduction–accretion of the Paleo–Pacific Plate;
3. Summarizing the rock association of subduction in the NAC belt, we hold the opinion that the initial age of subduction of the Paleo–Pacific Plate may be the Permian. The accretionary complexes in the NAC belt have a younging trend from west to east, indicating a westward subduction and accretion process of the Paleo–Pacific Ocean during the Permian to Early Cretaceous.

Supplementary Materials: The following supporting information can be downloaded at: https://www.mdpi.com/article/10.3390/min13081038/s1: Table S1: LA–ICP–MS U–Pb data of zircons from Tongjiang accretionary complex matrix; Table S2: Lu–Hf isotopic analyses of zircons from Tongjiang accretionary complex matrix.

Author Contributions: Writing–original draft preparation, B.D., C.L. and F.L.; writing—review and editing, T.L., Y.L (Yong Liu). and T.Z.; methodology, X.W.; investigation, B.D., Y.L. (Yuwei Liu) and T.Z. All authors have read and agreed to the published version of the manuscript.

Funding: This work is supported by the Bureau Geology and Mineral Resources of Heilongjiang Province (Project HKY202303), the China Geological Survey (Project DD20221645, DD20221630 and DD20230340) and the National Natural Science Foundation of China (Project 92062215, 41720104009).

Data Availability Statement: The authors confirm that the data supporting the findings of this study are available within the article and/or its Supplementary Materials.

Acknowledgments: We would like to thank the editors and anonymous reviewers for their constructive comments and suggestions, which led to significant improvements in the manuscript.

Conflicts of Interest: The authors declare no conflict of interest.

References

1. Matsuda, T.; Isozaki, Y. Well-documented travel history of Mesozoic pelagic chert in Japan. *Tectonics* **1991**, *10*, 475–499. [CrossRef]
2. Cawood, P.A.; Kröner, A.; Collins, W.J.; Kusky, T.M.; Mooney, W.D.; Windley, B.F. Accretionary Orogens Through Earth History. *Geol. Soc. Lond. Spec. Publ.* **2009**, *318*, 1–36. [CrossRef]
3. Kusky, T.M.; Windley, B.F.; Safonova, I.; Wakita, K.; Wakabayashi, J.; Polat, A.; Santosh, M. Recognition of ocean plate stratigraphy in accretionary orogens through Earth history:A record of 3.8 billion years of sea floor spreading, subduction, and accretion. *Gondwana Res.* **2013**, *24*, 501–547. [CrossRef]
4. Safonova, I.Y.; Santosh, M. Accretionary complexes in the Asia-Pacific region: Tracing archives of ocean plate stratigraphy and tracking mantle plumes. *Gondwana Res.* **2014**, *25*, 126–158. [CrossRef]
5. Xiao, W.J.; Li, J.L.; Song, D.F.; Han, C.M.; Wan, B.; Zhang, J.E.; AO, S.J.; Zhang, Z.Y. Structural analyses and spatio-temporal constraints of accretionary orogens. *Earth Sci.* **2019**, *44*, 1661–1687.
6. Zhou, J.B. Accretionary complex: Geological records from oceanic subduction to continental deep subduction. *Sci. China Earth Sci.* **2020**, *50*, 1709–1726. [CrossRef]
7. Yan, Z.; Fu, C.L.; Niu, M.L.; Zhang, J.E.; Xiao, W.J.; Wang, Z.Q. Recognition and significance of accretionary prism in orogenic belts. *Chin. J. Geol.* **2021**, *56*, 430–448.
8. Zhou, J.B.; Wilde, S.A.; Zhang, X.Z.; Zhao, G.C.; Zheng, C.Q.; Wang, Y.J.; Zhang, X.H. The onset of Pacific margin accretion in NE China: Evidence from the Heilongjiang high-pressure metamorphic belt. *Tectonophysics* **2009**, *478*, 230–246. [CrossRef]
9. Zhou, J.B.; Wilde, S.A. The crustal accretion history and tectonic evolution of the NE China segment of the Central Asian Orogenic Belt. *Gondwana Res.* **2013**, *23*, 1365–1377. [CrossRef]
10. Lan, H.Y.; Li, S.Z.; Guo, L.L.; Li, X.Y.; Liu, Y.J.; Liu, B.; Santosh, M.; Cao, X.Z.; Zhang, R.X.; Wang, G.Z. Mesozoic deformation of the Nadanhada Terrane and its implications on the subduction of the Paleo-Pacific Plate. *J. Asian Earth Sci.* **2022**, *232*, 105166. [CrossRef]
11. Li, S.Z.; Zhang, Y.; Guo, L.L.; Suo, Y.H.; Cao, H.H.; Li, X.Y.; Zhou, Z.Z.; Wang, P.C.; Guo, R.H. Mesozoic deformation and accretionary orogenic processes around the Nadanhada Terrane. *Earth Sci. Front.* **2017**, *24*, 200–212.
12. Zhou, J.B.; Pu, X.G.; Hou, H.S.; Han, W.; Cao, J.L.; Li, G.Y. The Mesozoic accretionary complex in NE China and its tectonic implications for the subduction of the Paleo-Pacific plate beneath the Eurasia. *Acta Petrol. Sin.* **2018**, *34*, 2845–2856.
13. Xu, W.L.; Sun, C.Y.; Tang, J.; Luan, J.P.; Wang, F. Basement nature and tectonic evolution of the Xing'an-Mongolian Orogenic Belt. *Earth Sci.* **2019**, *44*, 1620–1646.
14. Han, W.; Zhou, J.B. Paleo-Pacific subduction-accretion: Geochemical and geochronology constraints from the Raohe accretionary complex, NE China. *Acta Petrol. Sin.* **2020**, *36*, 703–725.
15. Xu, W.L.; Wang, Y.N.; Wang, F.; Tang, J.; Long, X.Y.; Dong, Y.; Li, Y.; Zhang, X.Z. Evolution of western Pacific subduction zones: Constraints from accretionary complexes in NE Asian continental margin. *Acta Palaeontol. Sin.* **2022**, *68*, 1–17.
16. Guo, F. Geological records of the Pacific plate subduction in the Northeast Asian continental margin: An overview. *Bull. Miner. Petrol Geochem.* **2016**, *35*, 1082–1089.
17. Wang, Z.H. The Mesozoic-Early Cenozoic Tectono-Magmatic Evolution of the Nadanhada Terrane. Ph.D. Thesis, Jilin University, Changchun, China, 2017.
18. Wang, Z.H.; Ge, W.C.; Yang, H.; Bi, J.H.; Ji, Z.; Dong, Y.; Xu, W.L. Petrogenesis and tectonic implications of Early Jurassic volcanic rocks of the Raohe accretionary complex, NE China. *J. Asian Earth Sci.* **2017**, *134*, 262–280. [CrossRef]
19. Tang, J.; Xu, W.L.; Wang, F.; Ge, W.C. Subduction history of the Paleo-Pacific slab beneath Eurasian continent: Mesozoic-Paleogene magmatic records in Northeast Asia. *Sci. China Earth Sci.* **2018**, *61*, 527–559. [CrossRef]
20. Zhou, J.B.; Cao, J.L.; Wilde, S.A.; Zhao, G.C.; Zhang, J.J.; Wang, B. Paleo-Pacific subduction-accretion: Evidence from Geochemical and U-Pb zircon dating of the Nadanhada accretionary complex, NE China. *Tectonics* **2014**, *33*, 2444–2466. [CrossRef]
21. Sun, M.D.; Xu, Y.G.; Wilde, S.A.; Chen, H.L.; Yang, S.F. The Permian Dongfanghong island-arc gabbro of the Wandashan Orogen, NE China: Implications for Paleo-Pacific subduction. *Tectonophysics* **2015**, *659*, 122–136. [CrossRef]

22. Yang, H.; Ge, W.C.; Dong, Y.; Bi, J.H.; Wang, Z.H.; Ji, Z. Record of Permian-Early Triassic continental arc magmatism in the western margin of the Jiamusi Block, NE China: Petrogenesis and implications for Paleo-Pacific subduction. *Int. J. Earth Sci.* **2017**, *106*, 1919–1942. [CrossRef]
23. Zhou, J.B.; Shi, A.G.; Jing, Y. The Combined NE China blocks:Tectonic evolution and supercontinent reconstructions. *J. Jilin Uni. Earth Sci. Ed.* **2016**, *46*, 1042–1055.
24. Khanchuk, A.I.; Kemkin, I.V.; Kruk, N.N. The Sikhote-Alin orogenic belt, Russian South East: Terranes and the formation of continental lithosphere based on geological and isotopic data. *J. Asian Earth Sci.* **2016**, *120*, 117–138. [CrossRef]
25. Zhou, J.B.; Li, L. The Mesozoic accretionary complex in Northeast China: Evidence for the accretion history of Paleo-Pacific subduction. *J. Asian Earth Sci.* **2017**, *145*, 91–100. [CrossRef]
26. Zheng, H.; Sun, X.M.; Wan, K.; Wang, P.J.; He, S.; Zhang, X.Q. Structure and tectonic evolution of the Late Jurassic-Early Cretaceous Wandashan accretionary complex, NE China. *Int. Geol. Rev.* **2019**, *61*, 17–38. [CrossRef]
27. Liang, Y.; Zheng, H.; Li, H.; Algeo, J.T.; Sun, X.M. Late Paleozoic–Mesozoic subduction and accretion of the Paleo-Pacific Plate: Insights from ophiolitic rocks in the Wandashan accretionary complex, NE China. *Geosci. Front.* **2021**, *12*, 101242. [CrossRef]
28. Golozubov, V.V.; Khanchuk, A.I. The Heilongjiang Complex as a Fragment of a Jurassic Accretionary Wedge in the Tectonic Windows of the Overlying Plate: A Flat Slab Subduction Model. *Russ. J. Pac. Geol.* **2021**, *40*, 3–17. [CrossRef]
29. Kojima, S. Mesozoic terrane accretion in Northeast China, Sikhote-Alin and Japan regions. *Palaeogeogr. Palaeocl.* **1989**, *69*, 213–232. [CrossRef]
30. Li, W.M.; Liu, Y.J.; Zhao, Y.L.; Feng, Z.Q.; Zhou, J.P.; Wen, Q.B.; Ling, C.Y.; Zhang, D. Tectonic evolution of the Jiamusi Block, NE China. *Acta Petrol. Sin.* **2020**, *36*, 665–684.
31. Wang, Y.N.; Xu, W.L.; Wang, F.; Zhang, X.Z. Late Paleozoic–Mesozoic tectonic evolution of the northeastern Asian continental margin revealed by sedimentary formations and fossil accretionary complexes. *Earth-Sci. Rev.* **2021**, *225*, 103908. [CrossRef]
32. Bi, J.H. Late Paleozoic Tectonic-Magmatic Evolution of the Eastern Jiamusi Massif. Ph.D. Thesis, Jilin University, Changchun, China, 2018.
33. Zeng, Z.; Zhang, X.Z.; Zhou, J.B.; Zhang, H.T.; Liu, Y.; Cui, W.L. Geochemistry and zircon U-Pb age of Permian metabasalts in the Yuejinshan complexes and its tectonic implications. *Geotecton. Metallog.* **2018**, *42*, 365–378.
34. Liu, Y.J.; Feng, Z.Q.; Jiang, L.W.; Jin, W.; Li, W.M.; Guan, Q.B.; Wen, Q.B.; Liang, C.Y. Ophiolite in the eastern Central Asian Orogenic Belt, NE China. *Acta Petrol. Sin.* **2019**, *35*, 3017–3047.
35. Zhang, D.; Liu, Y.J.; Li, W.M.; Li, S.Z.; Iqbal, M.Z.; Chen, Z.X. Marginal accretion processes of Jiamusi Block in NE China: Evidences from detrital zircon U-Pb age and deformation of the Wandashan Terrane. *Gondwana Res.* **2020**, *78*, 92–109. [CrossRef]
36. Cheng, R.Y.; Wu, F.Y.; Ge, W.C.; Sun, D.Y.; Yang, X.M.; Yang, J.H. Emplacement age of the Raohe Complex in eastern Heilongjiang Province and the tectonic evolution of the eastern part of Northeastern China. *Acta Petrol Sin.* **2006**, *22*, 353–376.
37. Zhang, D. Marginal Accretion Processes of Jiamusi Block in NE China: Evidences from Mesozoic Clastic Rocks of the Wandashan Terrane. Master's Thesis, Jilin University, Changchun, China, 2019.
38. Meng, E.; Xu, W.L.; Yang, D.B.; Pei, F.P.; Yu, Y.; Zhang, X.Z. Permian volcanisms in eastern and southeastern margins of the Jiamusi Massif, northeastern China: Zircon U–Pb chronology, geochemistry and its tectonic implications. *Chin. Sci. Bull.* **2008**, *53*, 1231–1245. [CrossRef]
39. Xu, W.L.; Wang, F.; Meng, E.; Gao, F.H.; Pei, F.P.; Yu, J.J.; Tang, J. Paleozoic-Early Mesozoic tectonic evolution in eastern Heilongjiang Province, NE China: Evidence from igneous rock association and U-Pb geochronology of detrital zircons. *J. Jilin Uni. Earth Sci. Ed.* **2012**, *42*, 1378–1389.
40. Li, G.Y.; Zhou, J.B.; Li, L. The Early Permian active continental margin at the eastern margin of the Jiamusi Block, NE China: Evidenced by zircon U–Pb chronology and geochemistry of the Erlongshan andesites. *Geol. J.* **2019**, *55*, 1670–1688. [CrossRef]
41. Li, G.Y.; Zhou, J.B.; Li, L. The Jiamusi Block: A hinge of the tectonic transition from the Paleo-Asian Ocean to the Paleo-Pacific Ocean regimes. *Earth Sci. Rev.* **2023**, *236*, 104279. [CrossRef]
42. Bi, J.H.; Ge, W.C.; Yang, H.; Zhao, G.C.; Xu, W.L.; Wang, Z.H. Geochronology, geochemistry and zircon Hf isotopes of the Dongfanghong gabbroic complex at the eastern margin of the Jiamusi Massif, NE China: Petrogensis and tectonic implications. *Lithos* **2015**, *234–235*, 27–46. [CrossRef]
43. Bi, J.H.; Ge, W.C.; Yang, H.; Wang, Z.H.; Xu, W.L.; Yang, J.H.; Xing, D.H.; Chen, H.J. Geochronology and geochemistry of late Carboniferous–middle Permian I-and A-type granites and gabbro–diorites in the eastern Jiamusi Massif, NE China: Implications for petrogenesis and tectonic setting. *Lithos* **2016**, *266–267*, 213–232. [CrossRef]
44. Bi, J.H.; Ge, W.C.; Yang, H.; Wang, Z.H.; Dong, Y.; Liu, X.W.; Ji, Z. Age, petrogenesis, and tectonic setting of the Permian bimodal volcanic rocks in the eastern Jiamusi Massif, NE China. *J. Asian Earth Sci.* **2017**, *134*, 160–175. [CrossRef]
45. Liu, K.; Zhang, J.J.; Ge, M.H.; Ling, Y.Y. Mesozoic Subduction of the Paleo-Pacific Plate along the eastern Margin of the Xing-Meng Orogenic Belt. *Bull. Miner. Petrol Geochem.* **2016**, *35*, 1098–1108.
46. Zeng, Z. The Tectonic Characteristics and Evolution of Jiamusi Massif and Wandashan Complex. Ph.D. Thesis, Jilin University, Changchun, China, 2017.
47. Cui, W.L. The Discovery and Significance of Permian Subducting Oceanic Crust on the eastern Margin of Jiamusi Massif, NE China. Master's Thesis, Jilin University, Changchun, China, 2018.
48. Wu, F.Y.; Yang, J.H.; Lo, C.H.; Wilde, S.A.; Sun, D.Y.; Jahn, B.M. The Heilongjiang group: A Jurassic accretionary complex in the Jiamusi Massif at the western Pacific margin of northeastern China. *Isl. Arc.* **2007**, *16*, 156–172. [CrossRef]

49. Feng, G.Y.; Dilek, Y.; Niu, X.L.; Liu, F.; Yang, J.S. Geochemistry and geochronology of OIB-type, Early Jurassic magmatism in the Zhangguangcai range, NE China, as a result of continental back-arc extension. *Geol. Mag.* **2021**, *158*, 143–157. [CrossRef]
50. BGMRHLJ (Bureau of Geology and Mineral Resources of Heilongjiang Province). *Regional Geology of the Heilongjiang Province*; Geological Publishing House: Beijing, China, 1993; pp. 1–734.
51. Wang, J.R.; Yang, Y.C.; Huang, Y.W.; Hou, Y.S.; Tan, Y.; Zhang, G.B. Fromation Ages and Tectonic Significance of Ophiolites in Wandashan Terrane of the Eastern Heilongjiang. *J. Earth Sci. Environ.* **2016**, *38*, 182–195.
52. Sun, M.D.; Xu, Y.G.; Wilde, S.A.; Chen, H.L. Provenance of Cretaceous trench slope sediments from the Mesozoic Wandashan Orogen, NE China: Implications for determining ancient drainage systems and tectonics of the Paleo-Pacific. *Tectonics* **2015**, *34*, 1269–1289. [CrossRef]
53. Zeng, Z.; Sun, L.; Zhang, X.Z.; Cui, W.L.; Jiang, L. Zircon U-Pb Chronology And Geochemistry of The Pillow Basalts From Raohe Complex: Geological Implications. *Geol. Resour.* **2019**, *28*, 119–127.
54. Sun, M.D.; Xu, Y.G.; Chen, H.L. Subaqueous volcanism in the Paleo-Pacific Ocean based on Jurassic basaltic tuff and pillow basalt in the Raohe Complex, NE China. *Sci. China Earth Sci.* **2018**, *48*, 1016–1032. [CrossRef]
55. Guo, Y. The Nature of the Yuejinshan Complex in the Eastern Part of Heilongjiang Province and Its Evolution. Ph.D. Thesis, Jilin University, Changchun, China, 2016.
56. Zhang, Q.L.; Mizutani, S.; Kojima, S.; Shao, J.A. The Nadanhada terrane in Heilongjiang Province. *Geol. Rev.* **1989**, *35*, 67–71.
57. Liu, C.; Zhang, X.Z.; Liu, Y.; Yang, B.J.; Feng, X.; Wang, D.; Liu, D.M. Geoelectrical evidence for characteristics of lithospheric structure beneath the Yuejinshan collage zone and its vicinity in Northeast Asia. *Chin. J. Geophys.* **2009**, *52*, 958–965. [CrossRef]
58. Zhang, Q.L.; Mizutani, S.; Kojima, S. Radiolaria and correlation study of terranes. *Acta Palaeontol. Sin.* **1997**, *36*, 245–252.
59. Shao, J.A.; Tang, K.D.; Wang, C.Y.; Zang, Q.J.; Zhang, Y.P. The tectonic characteristics and evolution of Nadanhada Terrane. *Sci. China Ser. B* **1991**, *7*, 744–751.
60. Ye, G.Y.; Yang, Q. Radiolarian Assemblages From T-J Boundary Strata, Nadanhada Terrane, NE China. *Acta Micropalaeontol. Sin.* **2006**, *23*, 317–360.
61. Tian, D.J.; Zhou, J.B.; Zheng, C.Q.; Liu, J.H. Geochemical characteristics and tectonics mechanism of the meta-basic rocks for ophiolite complex in Wandashan orogenic belt. *Miner. Petrol.* **2006**, *26*, 64–70.
62. Zong, K.Q.; Klemd, R.; Yuan, Y.; He, Z.Y.; Guo, J.L.; Shi, X.L.; Liu, Y.S.; Hu, Z.C.; Zhang, Z.M. The assembly of Rodinia: The correlation of early Neoproterozoic (ca. 900 Ma) high-grade metamorphism and continental arc formation in the southern Beishan Orogen, southern Central Asian Orogenic Belt (CAOB). *Precambrian Res.* **2017**, *290*, 32–48. [CrossRef]
63. Liu, Y.S.; Hu, Z.C.; Gao, S.; Günther, D.; Xu, J.; Gao, C.G.; Chen, H.H. In situ analysis of major and trace elements of anhydrous minerals by LA-ICP-MS without applying an internal standard. *Chem. Geol.* **2008**, *257*, 34–43. [CrossRef]
64. Liu, Y.S.; Gao, S.; Hu, Z.C.; Gao, C.G.; Zong, K.Q.; Wang, D.B. Continental and oceanic crust recycling-induced melt-peridotite interactions in the Trans-North China Orogen: U-Pb dating, Hf isotopes and trace elements in zircons of mantle xenoliths. *J Petrol.* **2010**, *51*, 537–571. [CrossRef]
65. Ludwig, K.R. *ISOPLOT 3.00: A Geochronological Toolkit for Microsoft Excel*; Berkeley Geochronology Center: Berkeley, CA, USA, 2003.
66. Hu, Z.C.; Liu, Y.S.; Gao, S.; Liu, W.G.; Yang, L.; Zhang, W.; Tong, X.R.; Lin, L.; Zong, K.Q.; Li, M.; et al. Improved in situ Hf isotope ratio analysis of zircon using newly designed X skimmer cone and Jet sample cone in combination with the addition of nitrogen by laser ablation multiple collector ICP-MS. *J. Anal. Atom. Spectrome.* **2012**, *27*, 1391–1399. [CrossRef]
67. Blichert-Toft, J.; Chauvel, C.; Albarède, F. Separation of Hf and Lu for high-precision isotope analysis of rock samples by magnetic sector-multiple collector ICP-MS. *Contrib. Mineral. Petr.* **1997**, *127*, 248–260. [CrossRef]
68. Fisher, C.M.; Vervoort, J.D.; Hanchar, J.M. Guidelines for reporting zircon Hf isotopic data by LA-MC-ICPMS and potential pitfalls in the interpretation of these data. *Chem. Geol.* **2014**, *363*, 125–133. [CrossRef]
69. Nelson, D.R. An assessment of the determination of depositional ages for precambrian clastic sedimentary rocks by U-Pb dating of detrital zircons. *Sediment. Geol.* **2001**, *141*, 37–60. [CrossRef]
70. Fedo, C.M.; Sircombe, K.N.; Rainbird, R.H. Detrital zircon analysis of the sedimentary record. *Rev. Mineral. Geochem.* **2003**, *53*, 277–303. [CrossRef]
71. Dickinson, W.R.; Gehrels, G.E. Use of U-Pb ages of detrital zircons to infer maximum depositional ages of strata: A test against a Colorado Plateau Mesozoic database. *Earth Planet. Sc. Lett.* **2009**, *288*, 115–125. [CrossRef]
72. Thomas, W.A. Detrital-Zircon Geochronology and Sedimentary Provenance. *Lithosphere* **2011**, *3*, 304–308. [CrossRef]
73. Cherniak, D.J.; Watson, E.B. Pb diffusion in zircon-ScienceDirect. *Chem. Geol.* **2001**, *172*, 5–24. [CrossRef]
74. Gao, F.H.; Yang, Y.; Wang, F.; Xu, W.L. De- termination of the Early Paleozoic strata in eastern Hei-longjiang Province: Evidence from field geology and de- trital zircon U-Pb geochronology. *Earth Sci.* **2014**, *39*, 499–508.
75. Wang, Z.H.; Ge, W.C.; Yang, H.; Zhang, Y.L.; Bi, J.H.; Tian, D.X.; Xu, W.L. Middle Jurassic oceanic island igneous rocks of the Raohe accretionary complex, northeastern China: Petrogenesis and tectonic implications. *J. Asian Earth Sci.* **2015**, *111*, 120–137. [CrossRef]
76. Wang, F.; Xu, Y.G.; Xu, W.L.; Yang, L.; Wu, W.; Sun, C.Y. Early Jurassic talc-alkaline magmatism in northeast China: Magmatic response to subduction of the Paleo-Pacific Plate beneath the Eurasian continent. *J. Asian Earth Sci.* **2017**, *143*, 249–268. [CrossRef]

77. Liu, K.; Zhang, J.J.; Wilde, S.A.; Zhou, J.B.; Wang, M.; Ge, M.H.; Wang, J.M.; Ling, Y.Y. Initial subduction of the Paleo-Pacific Oceanic plate in NE China: Constraints from whole-rock geochemistry and zircon U-Pb and Lu-Hf isotopes of the Khanka Lake granitoids. *Lithos* **2017**, *274*, 254–270. [CrossRef]
78. Wu, F.Y.; Wilde, S.A.; Sun, D.Y. Zircon SHRIMP U-Pb ages of gneissic granites in Jiamusi massif, northeastern China. *Acta Petrol. Sin.* **2001**, *17*, 443–452.
79. Bi, J.H.; Ge, W.C.; Zhang, Y.L.; Yang, H.; Wang, Z.H. Petrogenesis of Permian Jinshan granitic complex in the eastern Jiamusi Massif and its geological implications. *J. Earth Sci. Environ.* **2014**, *36*, 16–31.
80. Yang, H.; Ge, W.C.; Zhao, G.C.; Yu, J.J.; Zhang, Y.L. Early Permian-Late Triassic granitic magmatism in the Jiamusi-Khanka Massif, eastern segment of the Central Asian Orogenic Belt and its implications. *Gondwana Res.* **2015**, *27*, 1509–1533. [CrossRef]
81. Dong, Y.; Ge, W.C.; Yang, H.; Bi, J.H.; Wang, Z.H.; Xu, W.L. Permian tectonic evolution of the Mudanjiang Ocean: Evidence from zircon U-Pb-Hf isotopes and geochemistry of a N-S trending granitoid belt in the Jiamusi Massif, NE China. *Gondwana Res.* **2017**, *49*, 147–163. [CrossRef]
82. Meng, E. Late Paleozoic-Early Mesozoic Tectonic Evolution in the Eastern Heilongjiang Province, NE China: Constrains from Detrital Zircons and Volcanical Events. Ph.D. Thesis, Jilin University, Changchun, China, 2011.
83. Bi, J.H.; Ge, W.C.; Yang, H.; Zhao, G.C.; Yu, J.J.; Zhang, Y.L.; Wang, Z.H.; Tian, D.X. Petrogenesis and tectonic implications of early Paleozoic granitic magmatism in the Jiamusi Massif, NE China: Geochronological, geochemical and Hf isotopic evidence. *J. Asian Earth Sci.* **2014**, *96*, 308–331. [CrossRef]
84. Yang, H. Research on the Neoproterozoic-Early Paleozoic Tectono-Magmatic Events in the Jiamusi Block. Ph.D. Thesis, Jilin University, Changchun, China, 2017.
85. Zheng, T.; Qian, Y.; Shen, Y.J.; Tian, S.N.; Zhao, C.J.; Xiu, Y.M.; Sun, F.Y. Mineralization age, tectonic setting and ore genesis of the Wuxing Pt-Pd-rich magmatic Cu-Ni sulfide deposit, Northeast China. *Ore Geol. Rev.* **2021**, *134*, 104189. [CrossRef]
86. Lü, C.L.; Feng, J.L.; Zheng, W.Z.; Ren, F.H.; Wang, Q.M. Zircon dating and its geological significance of homblende-biotite granite gneisses in Jiamusi Massif: The clue comes from the Neoproterozoic basement. *China Min. Mag.* **2014**, *23* (Suppl. 2), 127–132.
87. Yang, H.; Ge, W.C.; Zhao, G.C.; Dong, Y.; Xu, W.L.; Ji, Z.; Yu, J.J. Late Triassic intrusive complex in the Jidong region, Jiamusi-Khanka Block, NE China: Geochemistry, zircon U-Pb ages, Lu-Hf isotopes, and implications for magma mingling and mixing. *Lithos* **2015**, *224–225*, 143–159. [CrossRef]
88. Han, S.J.; Yang, Y.C.; Bo, J.W.; Zhang, G.B.; Khomich, V.G.; Huang, Y.W.; Yang, Y.B.; Wang, X.Y. Late Neoarchean magmatic record of the Jiamusi-Khanka Block, Northeast China: New clues from amphibolite zircon U-Pb geochronology and Lu-Hf isotopes. *Geol. J.* **2020**, *55*, 3401–3415. [CrossRef]
89. Zhang, X.J.; Takeuchi, M.; Ohkawa, M.; Matsuzawa, N. Provenance of a Permian accretionary complex (Nishiki Group) of the Akiyoshi Belt in Southwest Japan and Paleogeographic implications. *J. Asian Earth Sci.* **2018**, *167*, 130–138. [CrossRef]
90. Yang, J.H.; Wu, F.Y.; Shao, J.; Wilde, S.A.; Xie, L.W.; Liu, X.M. Constraints on the timing of uplift of the Yanshan Fold and Thrust Belt, North China. *Earth Planet. Sci. Lett.* **2006**, *246*, 336–352. [CrossRef]
91. BGMRHLJ (Bureau of Geology and Mineral Resources of Heilongjiang Province). *Stratigraphy (Lithostratic) of Heilongjiang Province*; China University of Geosciences Press: Wuhan, China, 1997; pp. 1–298.
92. Luan, J.P.; Wang, F.; Xu, W.L.; Ge, W.C.; Sorokin, A.A.; Wang, Z.W.; Guo, P. Provenance, age, and tectonic implications of Neoproterozoic strata in the Jiamusi Massif: Evidence from U-Pb ages and Hf isotope compositions of detrital and magmatic zircons. *Precambrian Res.* **2017**, *297*, 19–32. [CrossRef]
93. Yang, Z.; Liang, H.D.; Gao, R.; Bi, H.; Zhou, J.B.; Xin, Z.H.; Lu, A.R. Lithospheric electrical structure of the southern segment of the Jiamusi massif and its adjacent areas revealed by 3D magnetotelluric inversion. *Chin. J. Geophys.* **2022**, *65*, 4383–4393.
94. Reagan, M.K.; Ishizuka, O.; Stern, R.J.; Kelley, K.A.; Ohara, Y.; Blichert-Toft, J.; Bloomer, S.H.; Cash, J.; Fryer, P.; Hanan, B.B.; et al. Fore-arc basalts and subduction initiation in the Izu- Bonin-Mariana system. *Geochem. Geophy. Geosy.* **2010**, *11*, 1–17. [CrossRef]
95. Ishizuka, O.; Kimura, J.I.; Li, Y.B.; Stern, R.J.; Reagan, M.K.; Taylor, R.N.; Ohara, Y.; Bloomer, S.H.; Ishii, T.; Hargrove, U.S., III; et al. Early stages in the evolution of Izu- Bonin arc volcanism: New age, chemical, and isotopic constraints. *Earth Planet. Sci. Lett.* **2006**, *250*, 385–401. [CrossRef]
96. Ishizuka, O.; Tani, K.; Reagan, M.K. KIzu-Bonin-Mariana forearc crust as a modern ophiolite analogue. *Elements* **2014**, *10*, 115–120. [CrossRef]
97. Deng, J.F.; Liu, C.; Feng, Y.F.; Xiao, Q.H.; Su, S.G.; Zhao, G.C.; Kong, W.Q.; Cao, W.Y. High magnesian andesitic/dioritic rocks (HMA) and magnesian andesitic/dioritic rocks (MA): Two igneous rock types related to oceanic subduction. *Geol. China* **2010**, *37*, 1112–1118.
98. Xiao, Q.H.; Li, T.D.; Pang, G.T.; Lu, S.N.; Ding, X.Z.; Deng, J.F.; Feng, Y.M.; Liu, Y.; Kou, C.H.; Yang, L.L. Petrologic ideas for identification of ocean-continent transition: Recognition of intra-oceanic arc and initial subduction. *Geol. China* **2016**, *43*, 721–737.
99. Du, B.Y.; Liu, F.; Liu, Y.; Liu, Y.W.; Gao, H.Y.; Zhen, M.; Zhang, T.A. Permian-Early Jurassic ocean-continent evolution and metallogenic dynamic setting in the central and eastern part of Heilongjiang Province. *Geol. Rev.* **2022**, *68*, 431–451.
100. Jing, Y.; Yang, H.; Ge, W.C.; Dong, Y.; Ji, Z.; Bi, J.H.; Zhou, H.Y.; Xing, D.H. When did the final closure occur of the eastern Paleo-Asian Ocean: Constraints from the latest Early–Middle Triassic adakitic granites in the southeastern Central Asian Orogenic Belt. *Gondwana Res.* **2022**, *103*, 146–171. [CrossRef]

101. Wakita, K.; Chen, Y.C.; Zhang, J.E.; Wang, J.P. Concept of OPS mélange and its field mapping technique for ancient accretionary complexes: Using some examples mainly from Jurassic accretionary complexes of the Mino and Chichibu belts in Japan. *Chin. J. Geol.* **2021**, *56*, 395–429.
102. Liu, F.; Yang, J.S.; Feng, G.Y.; Niu, X.L.; Li, G.L.; Zhang, C.F. Late Permian to Early Triassic subduction and retreating of the Paleopacific slab: Constraints from continental arc magmatism in Hainan Island. *Acta Petrol. Sin.* **2022**, *38*, 3455–3483.
103. Kemkin, I.V.; Khanchuk, A.I.; Kemkina, R.A. Accretionary prisms of the Sikhote-Alin Orogenic Belt: Composition, structure and significance for reconstruction of the geodynamic evolution of the eastern Asian margin. *J. Geodyn.* **2016**, *102*, 202–230. [CrossRef]
104. Kemkin, I.V.; Khanchuk, A.I.; Kemkina, R.A. Geochemistry of the Samarka terrane cherts (Sikhote-Alin) and the size of the accreted paleo-oceanic plate. *Russ. Geol. Geophys.* **2018**, *59*, 111–122. [CrossRef]

Disclaimer/Publisher's Note: The statements, opinions and data contained in all publications are solely those of the individual author(s) and contributor(s) and not of MDPI and/or the editor(s). MDPI and/or the editor(s) disclaim responsibility for any injury to people or property resulting from any ideas, methods, instructions or products referred to in the content.